RSC Advances

REVIEW

View Article Online
View Journal | View Issue

Open Access Article. Published on 23 October 2025. Downloaded on 10/25/2025 7:28:42 PM.
This article is licensed under a Creative Commons Attribution 3.0 Unported Licence.

Check for updates

Cite this: *RSC Adv.*, 2025, **15**, 40338

Pioneering perovskite quantum dot nanosensors for heavy metal ion detection: mechanisms, design, and industrial applications

Suleiman Ibrahim Mohammad,[ab] Asokan Vasudevan,[cd] I. B. Sapaev,[efgh] Munthar Kadhim Abosaoda,[ij] Chou-Yi Hsu,[k] Malatesh Akkur,[l] Alok Kumar Mishra,[m] Gaganjot Kaur,[n] Rajesh Singh[o] and Ahmad Mohebi *[p]

Perovskite quantum dots (PQDs) are a transformative platform for ultrasensitive heavy metal ion detection, leveraging high photoluminescence quantum yield (PLQY, 50–90%), narrow emission spectra (FWHM 12–40 nm), tunable bandgaps, and defect-tolerant optoelectronic properties. This review is the first systematic evaluation of PQD-based nanosensors for detecting Hg^{2+}, Cu^{2+}, Cd^{2+}, Fe^{3+}, Cr^{6+}, and Pb^{2+}, elucidating key mechanisms like cation exchange, electron/hole transfer, Förster resonance energy transfer, and surface trap-mediated quenching. Advanced synthesis methods, including hot-injection, ligand-assisted reprecipitation, and microwave-assisted techniques, enable precise control over size, crystallinity, and surface chemistry. Lead-based PQDs (*e.g.*, $CsPbX_3$) achieve limits of detection (LODs) as low as 0.1 nM with rapid response times (<10 s), while lead-free variants (*e.g.*, $Cs_3Bi_2X_9$, $CsSnX_3$) offer eco-friendly alternatives with enhanced aqueous stability. PQD@MOF composites and ratiometric designs enhance selectivity in complex matrices, surpassing carbon quantum dots and semiconductor QDs in sensitivity and versatility. Applications include industrial wastewater remediation, lubricant quality control, and environmental compliance, ensuring ecosystem protection and product integrity. This seminal work addresses challenges like aqueous instability, Pb toxicity, scalability, and matrix interference, benchmarking PQDs against alternative nanomaterials. Future directions include comparisons with other nanoparticles, multiplexed sensing platforms, and sustainable lead-free innovations. By integrating fundamental insights with practical applications, this review establishes PQDs as a high-impact paradigm for advancing heavy metal ion sensing in industrial and environmental contexts, guiding innovations in sensitivity, selectivity, and scalability.

Received 21st August 2025
Accepted 16th October 2025

DOI: 10.1039/d5ra06200d

rsc.li/rsc-advances

[a]*Electronic Marketing and Social Media, Economic and Administrative Sciences, Zarqa University, Jordan*
[b]*Research Follower, INTI International University, 71800 Negeri Sembilan, Malaysia*
[c]*Faculty of Business and Communications, INTI International University, 71800 Negeri Sembilan, Malaysia*
[d]*Shinawatra University, 99 Moo 10, Bangtoey, Samkhok, Pathum Thani 12160, Thailand*
[e]*Head of the Department Physics and Chemistry, "Tashkent Institute of Irrigation and Agricultural Mechanization Engineers" National Research University, Tashkent, Uzbekistan*
[f]*Scientific Researcher of the University of Tashkent for Applied Science, Uzbekistan*
[g]*School of Engineering, Central Asian University, Tashkent 111221, Uzbekistan*
[h]*Western Caspian University, Scientific Researcher, Baku, Azerbaijan*
[i]*College of Pharmacy, The Islamic University, Najaf, Iraq*
[j]*Department of Medical Analysis, Medical Laboratory Technique College, The Islamic University of Al Diwaniyah, Al Diwaniyah, Iraq*
[k]*Department of Pharmacy, Chia Nan University of Pharmacy and Science, Tainan 71710, Taiwan*
[l]*Department of Physics & Electronics, School of Sciences, JAIN (Deemed to be University), Bangalore, Karnataka, India*
[m]*Department of Electrical & Electronics Engineering, Siksha 'O' Anusandhan (Deemed to be University), Bhubaneswar, Odisha 751030, India*
[n]*Department of Electronics and Communication Engineering, Chandigarh University, Mohali, Punjab, India*
[o]*Uttaranchal Institute of Technology, Uttaranchal University, Dehradun 248007, Uttarakhand, India*
[p]*Department of Chemistry, Young Researchers and Elite Club, Islamic Azad University, Tehran Branch, Tehran, Iran. E-mail: a.mohebiacademic@gmail.com*

Ahmad Mohebi is a researcher in the Department of Chemistry, Young Researchers and Elite Club, Tehran Branch, Islamic Azad University, Tehran, Iran. He specializes in nanomaterials and sensor development, focusing on perovskite quantum dots for heavy metal ion detection in environmental and industrial applications. Mohebi leads interdisciplinary projects on sustainable nanotechnology, advancing sensor designs for wastewater and lubricant monitoring.

© 2025 The Author(s). Published by the Royal Society of Chemistry

Open Access Article. Published on 23 October 2025. Downloaded on 10/25/2025 7:28:42 PM.
This article is licensed under a Creative Commons Attribution 3.0 Unported Licence.

1. Introduction

Heavy metal ion contamination in environmental, industrial, and biological systems poses significant risks to ecosystems, human health, and industrial processes due to their toxicity, persistence, and bioaccumulation.[1–3] Elements such as mercury (Hg^{2+}), copper (Cu^{2+}), cadmium (Cd^{2+}), iron (Fe^{3+}), chromium (Cr^{6+}), and lead (Pb^{2+}) are prevalent pollutants in industrial wastewater, lubricants, and natural water bodies, necessitating robust detection methods to ensure environmental compliance and product integrity.[4–6] Traditional sensing technologies, including atomic absorption spectroscopy,[7,8] inductively coupled plasma mass spectrometry,[9,10] and electrochemical methods,[11,12] offer high sensitivity but are often hindered by high costs, complex instrumentation, and limited portability, making them less suitable for real-time or on-site applications.[13,14] In response, nanomaterial-based nanosensors have emerged as promising alternatives, offering rapid response, portability, and cost-effectiveness.[15] Among these, perovskite quantum dots (PQDs) have garnered significant attention due to their exceptional optoelectronic properties, positioning them as a transformative platform for heavy metal ion detection.[16,17]

PQDs, characterized by the general formula ABX_3 (where A is a monovalent cation, B is a divalent metal cation, and X is a halide anion), exhibit unique attributes that make them ideal for sensing applications.[18,19] Their high photoluminescence quantum yield (PLQY, 50–90%), narrow emission spectra (full width at half maximum (FWHM) 12–40 nm), and tunable bandgaps enable ultrasensitive detection with high color purity and specificity. These properties arise from quantum confinement effects at nanoscale dimensions (2–10 nm), which result in discrete energy levels and enhanced oscillator strengths.[20,21] Additionally, PQDs possess large absorption coefficients (10^5 to 10^6 cm^{-1}) and fast radiative recombination rates, facilitating efficient light harvesting and stable fluorescence signals critical for detecting analyte-induced changes. The structural versatility of PQDs allows compositional tuning through substitutions at the A, B, or X sites, enabling tailored optical and electronic properties for specific sensing needs.[19,20] Lead-based PQDs, such as $CsPbX_3$ and $CH_3NH_3PbX_3$, are renowned for their superior PLQY and tunable emission across the visible spectrum, while lead-free variants, such as $Cs_3Bi_2X_9$ and $CsSnX_3$, address toxicity concerns, offering eco-friendly alternatives with improved stability in aqueous environments.[22]

The detection of heavy metal ions using PQDs relies on their ability to undergo fluorescence quenching or enhancement triggered by interactions with analytes. Mechanisms such as cation exchange, electron transfer, and Förster Resonance Energy Transfer (FRET) underpin these responses, driven by the high surface-to-volume ratio and defect-tolerant nature of PQDs.[23,24] For instance, the ionic radius similarity between Pb^{2+} and Hg^{2+} facilitates rapid cation exchange in lead-based PQDs, leading to efficient quenching, while electron transfer dominates in interactions with transition metal ions like Cu^{2+} or Fe^{3+}.[17,21] Surface ligands, such as oleylamine or poly(-ethylenimine) (PEI), play a critical role in modulating selectivity and sensitivity by passivating defects and mediating ion–PQD interactions. Advanced synthesis methods, including hot-injection, ligand-assisted reprecipitation, and microwave-assisted techniques, enables precise control over PQD size, crystallinity, and surface chemistry, directly impacting their sensing performance.[25]

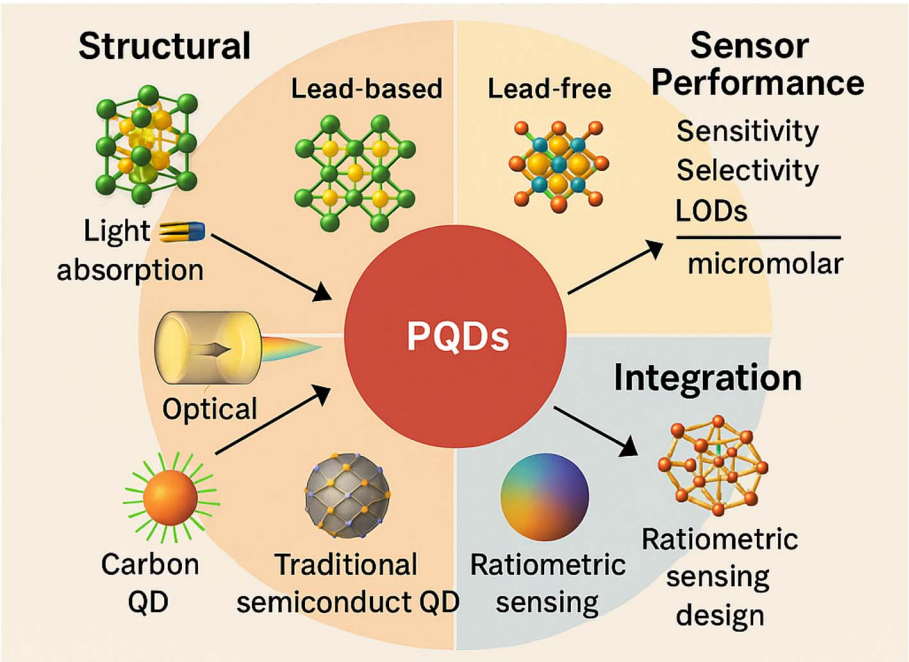

Fig. 1 Overview of PQD-based nanosensors for heavy metal ion detection, highlighting structure, performance, integration strategies, and comparison with other quantum dots.

Open Access Article. Published on 23 October 2025. Downloaded on 10/25/2025 7:28:42 PM. This article is licensed under a Creative Commons Attribution 3.0 Unported Licence.

The industrial relevance of PQD-based nanosensors lies in their ability to address critical monitoring needs in sectors such as chemical processing, wastewater treatment, and lubricant quality control.[26,27] Their high sensitivity and rapid response times make them suitable for detecting trace contaminants in real-time, ensuring compliance with stringent environmental regulations and maintaining product quality. However, challenges such as the aqueous instability of lead-based PQDs, toxicity concerns, and scalability of synthesis methods must be addressed to facilitate widespread adoption. Emerging strategies, including the development of lead-free PQDs, advanced encapsulation techniques, and computational modeling, offer pathways to overcome these limitations, paving the way for practical implementation.[28,29]

This review provides the first comprehensive analysis of PQD-based nanosensors for heavy metal ion detection, systematically exploring their structural, optical, and mechanistic foundations. It covers diverse PQD types, including lead-based (*e.g.*, $CsPbBr_3$) and lead-free (*e.g.*, $Cs_3Bi_2Br_9$) systems, their synthesis methods, and their advantages and limitations for sensing applications. The review evaluates sensor performance, focusing on sensitivity, selectivity, and limits of detection (LODs) ranging from sub-nanomolar (*e.g.*, 0.1 nM for Cu^{2+} in organic solvents) to micromolar levels, depending on the ion and matrix. Integration with stable matrices like metal–organic frameworks and ratiometric sensing designs enhances performance in complex industrial and environmental matrices. By comparing PQDs with other nanomaterials, such as carbon QDs and traditional semiconductor quantum dots, and addressing both fundamental and applied aspects, this work aims to guide future research, fostering innovations to improve the sensitivity, selectivity, and scalability of PQD-based nanosensors for diverse heavy metal ion detection applications (Fig. 1).

2. Fundamentals of perovskite quantum dots

2.1. Structural and optical properties of perovskite quantum dots

PQDs are nanoscale semiconductor materials characterized by the general formula ABX_3, where A is a monovalent cation (*e.g.*, Cs^+, methylammonium (MA^+), or formamidinium (FA^+)), B is a divalent metal cation (*e.g.*, Pb^{2+}, Sn^{2+}, or bismuth (Bi^{3+})), and X is a halide anion (*e.g.*, Cl^-, Br^-, or I^-). The crystal structure of PQDs typically adopts a cubic, tetragonal, or orthorhombic lattice in 3D ABX_3 forms, depending on the composition and temperature.[30,31] In this 3D structure, the B cation is coordinated octahedrally by six X anions, forming interconnected $[BX_6]^{4-}$ octahedra that create a three-dimensional framework, with A cations occupying cuboctahedral voids for charge neutrality. This extended connectivity enables efficient charge transport and high PLQY (50–90%). In contrast, 0D/2D derivatives like $A_3B_2X_9$ (*e.g.*, $Cs_3Bi_2X_9$) feature isolated $[B_2X_9]^{3-}$ dimers or layered structures with reduced octahedral connectivity, resulting in stronger quantum confinement, broader emission spectra (FWHM ~40–60 nm), and typically lower PLQY (20–50%), which impacts sensitivity in sensing applications due to increased defect states.[19,28,40] The structural versatility of perovskites enables compositional tuning at A, B, or X sites to modulate properties critical for heavy metal ion detection.

The stability of the perovskite lattice is governed by the Goldschmidt tolerance factor (t), defined as:

$$t = \frac{r_A + r_X}{\sqrt{2}(r_B + r_X)} \quad (1)$$

where r_A, r_B, and r_X are the ionic radii of A, B, and X ions, respectively. A tolerance factor between 0.8 and 1.0 ensures a stable 3D cubic structure, while lower values favor 0D/2D phases. For instance, $CsPbBr_3$ ($t \approx 0.81$) adopts a cubic 3D structure at room temperature, offering high optical efficiency, whereas $Cs_3Bi_2Br_9$ ($t < 0.8$) forms a 0D layered structure, enhancing aqueous stability but reducing radiative efficiency.[32,33,43]

The optical properties of PQDs are dominated by quantum confinement effects due to their nanoscale dimensions (2–10 nm), resulting in discrete energy levels and size-dependent bandgaps. This confinement enhances oscillator strength, leading to high PLQY (50–90% for 3D ABX_3; 20–50% for 0D/2D $A_3B_2X_9$) and narrow emission spectra (FWHM 12–40 nm for 3D; broader for 0D/2D). For example, 3D $CsPbBr_3$ emits green light at ~520 nm with FWHM ~20 nm, ideal for selective sensing, while 0D $Cs_3Bi_2Br_9$ shows blue emission (~450 nm) with higher stability in polar media.[15,26,43] The bandgap can be tuned by size or halide composition; smaller PQDs or Cl-rich 3D variants exhibit wider bandgaps (~3.0 eV for $CsPbCl_3$), while I-rich 3D forms have narrower ones (~1.7 eV for $CsPbI_3$). 0D/2D structures often display wider effective bandgaps due to confinement. PQDs possess large absorption coefficients (10^5 to 10^6 cm^{-1}) and fast radiative recombination rates, with defect tolerance minimizing non-radiative losses—more pronounced in 3D forms where defects lie within bands.[30,34]

The surface chemistry of PQDs significantly influences their properties. PQDs are capped with ligands like oleylamine (OAm) or oleic acid (OA), which passivate defects and enhance stability. In 3D ABX_3, ligands primarily provide steric protection, while in 0D/2D $A_3B_2X_9$, they also mitigate interlayer defects for better aqueous sensing.[18,35] Exciton dynamics in PQDs feature short radiative lifetimes (1–10 ns) and high binding energies (20–100 meV), enabling sensitive energy transfer for detection. The high surface-to-volume ratio amplifies ion interactions, with 0D/2D structures showing enhanced trap states for quenching but potentially slower kinetics compared to 3D forms.[14,36]

2.1.1. Crystal structure and compositional flexibility. A tolerance factor between 0.8 and 1.0 typically ensures a stable cubic perovskite structure, while deviations may lead to tetragonal or orthorhombic phases, impacting optical and sensing performance. For instance, $CsPbBr_3$ adopts a cubic structure at room temperature, offering high symmetry and optical efficiency, whereas $CH_3NH_3PbBr_3$ may transition to a tetragonal phase under certain conditions, affecting its photoluminescence stability.[32,33] The ability to substitute halides (*e.g.*, Cl^- for Br^-) or cations (*e.g.*, Sn^{2+} for Pb^{2+}) allows precise

 © 2025 The Author(s). Published by the Royal Society of Chemistry

Open Access Article. Published on 23 October 2025. Downloaded on 10/25/2025 7:28:42 PM.
This article is licensed under a Creative Commons Attribution 3.0 Unported Licence.

control over the lattice parameters, enabling tailored bandgap energies and emission properties.

2.1.2. Quantum confinement and optical properties. The optical properties of PQDs are dominated by quantum confinement effects due to their nanoscale dimensions (2–10 nm), which result in discrete energy levels and size-dependent bandgaps. This confinement enhances the oscillator strength, leading to high photoluminescence quantum yields (PLQY), often exceeding 50–90%, and narrow emission spectra with full width at half maximum (FWHM) values of 12–40 nm. For example, $CsPbBr_3$ PQDs emit green light at ∼520 nm with a FWHM of ∼20 nm, ensuring high color purity ideal for sensing applications.[15,26] The bandgap can be tuned by adjusting the particle size or halide composition; smaller PQDs or those with higher Cl content exhibit wider bandgaps (*e.g.*, ∼3.0 eV for $CsPbCl_3$), while larger PQDs or I-rich compositions have narrower bandgaps (*e.g.*, ∼1.7 eV for $CsPbI_3$). PQDs possess large absorption coefficients (10^5 to 10^6 cm^{-1}), enabling efficient light harvesting, and fast radiative recombination rates due to their direct bandgap nature. Their high defect tolerance, where defect states often lie within the conduction or valence bands rather than the bandgap, minimizes non-radiative recombination, enhancing PL efficiency.[30,34] This property is critical for sensing, as it ensures strong and stable fluorescence signals responsive to analyte-induced changes, such as quenching or enhancement.

Panel (a) demonstrates the PLQY of PQDs as a function of ligand amount (10^4 v/v%), comparing solution and film states, with PLQY values reaching up to 90%, reflecting the high oscillator strength and quantum confinement effects due to their nanoscale dimensions (2–10 nm).[20] This high PLQY, often exceeding 50–90%, is attributed to the discrete energy levels and size-dependent bandgaps, enhancing color purity with narrow emission spectra (FWHM 12–40 nm). Panel (b) presents time-resolved PL decay curves for pristine PQDs and those treated with PLAP at concentrations of 5×10^3, 1×10^3, and 2×10^3 v/v%, showing varied decay rates, which indicate tunable radiative recombination influenced by ligand-induced changes, aligning with the fast recombination rates and high absorption coefficients (10^5 to 10^6 cm^{-1}) typical of direct bandgap PQDs. Panel (c) displays PL spectra of PQDs at temperatures of 100 °C, 120 °C, 140 °C, 160 °C, and 180 °C, with emission peaks ranging from 493 to 530 nm, illustrating how temperature affects the bandgap and emission intensity due to quantum confinement and defect tolerance, where defect states within the bands minimize non-radiative recombination for stable fluorescence.[21] The narrow FWHM (∼20 nm for $CsPbBr_3$ at ∼520 nm) ensures high color purity, critical for sensing applications.

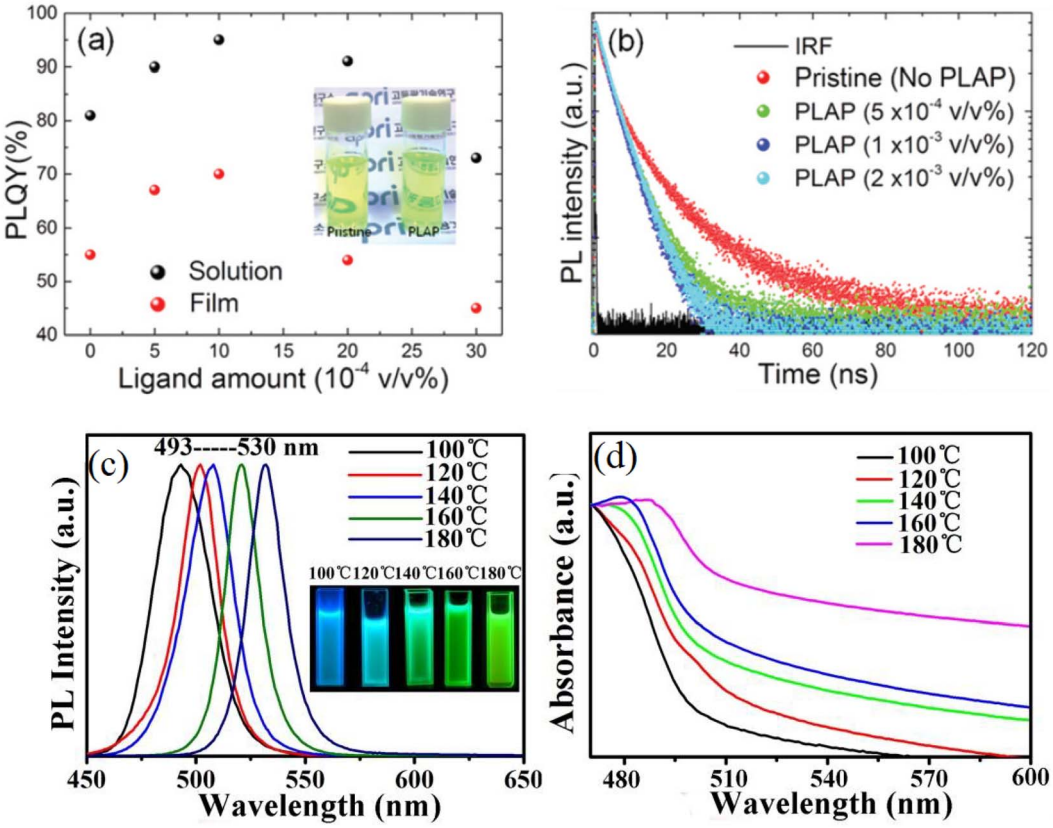

Fig. 2 (a) PLQY of PQDs as a function of ligand amount in solution and film, (b) time-resolved PL decay curves for pristine PQDs and PLAP-treated PQDs at different concentrations. Reprinted with permission from ref. 20. Copyright 2018, Royal Society of Chemistry. (c) PL spectra of PQDs at various temperatures, and (d) absorbance spectra of PQDs at different temperatures. Adapted with permission from ref. 21. Copyright 2017, Elsevier.

Open Access Article. Published on 23 October 2025. Downloaded on 10/25/2025 7:28:42 PM.
This article is licensed under a Creative Commons Attribution 3.0 Unported Licence.

Panel (d) shows absorbance spectra under the same temperature conditions, revealing shifts in the absorption edge (*e.g.*, ~3.0 eV for $CsPbCl_3$ to ~1.7 eV for $CsPbI_3$) due to size or halide composition tuning, highlighting the large absorption coefficients and efficient light harvesting, which support responsive fluorescence signals for analyte detection (Fig. 2).

2.1.3. Surface chemistry and ligand effects. The surface chemistry of PQDs significantly influences their optical and sensing properties. PQDs are typically capped with organic ligands, such as oleylamine (OAm) or oleic acid (OA), which passivate surface defects, enhance colloidal stability, and prevent aggregation. The ligand type and density affect the PLQY and environmental stability. For instance, long-chain ligands like OAm provide steric stabilization but may hinder analyte access in sensing applications, reducing sensitivity. Conversely, shorter or zwitterionic ligands can improve ion accessibility while maintaining stability in polar media.[18,35] Surface defects, if unpassivated, can act as non-radiative recombination centers, lowering PLQY and affecting sensing selectivity.[33] Ligand exchange strategies, such as replacing OAm with zwitterionic molecules, have been explored to enhance water compatibility for aqueous sensing.

2.1.4. Exciton dynamics and sensing relevance. The exciton dynamics in PQDs, characterized by short radiative lifetimes (1–10 ns) and high exciton binding energies (20–100 meV), contribute to their sensitivity in sensing applications. The strong excitonic effects enable efficient energy transfer mechanisms, such as FRET or electron transfer, when PQDs interact with metal ions. For example, the presence of heavy metal ions like Cu^{2+} or Hg^{2+} can induce fluorescence quenching through electron transfer or ion exchange, providing a measurable signal for detection.[14,36] The high surface-to-volume ratio of PQDs amplifies these interactions, making them highly responsive to low analyte concentrations, often achieving LOD in the nanomolar range.

2.2. Types of perovskite quantum dots

PQDs can be broadly classified into lead-based and lead-free variants, each with distinct structural, optical, and practical characteristics. Lead-based PQDs, such as $CsPbX_3$ and $CH_3NH_3PbX_3$, are the most studied due to their superior optical properties, while lead-free PQDs, such as $Cs_3Bi_2X_9$ and $CsSnX_3$, are gaining attention for their reduced toxicity and environmental compatibility.[31,37]

2.2.1. Lead-based perovskite quantum dots. Lead-based PQDs, including inorganic $CsPbX_3$ (X = Cl, Br, I) and organic–inorganic hybrids like $CH_3NH_3PbX_3$ or $FAPbX_3$, are renowned for their high PLQY (up to 90%), narrow emission spectra, and tunable bandgaps (1.7–3.0 eV). The lead cation (Pb^{2+}) in the B-site contributes to strong spin–orbit coupling, resulting in a direct bandgap and efficient radiative recombination. $CsPbX_3$ PQDs are fully inorganic, offering enhanced thermal and chemical stability compared to hybrids. For example, $CsPbBr_3$ exhibits robust green emission (~520 nm) and is widely used for detecting ions like Cu^{2+} and Cd^{2+} due to its high sensitivity to quenching mechanisms.[38] Organic–inorganic hybrids, such as $CH_3NH_3PbBr_3$, incorporate organic cations like methylammonium, which increase lattice flexibility but reduce stability under moisture or heat due to the volatility of the organic component. The halide composition in lead-based PQDs enables precise optical tuning, with $CsPbCl_3$ emitting blue (410 nm), $CsPbBr_3$ green, and $CsPbI_3$ red (680 nm). Mixed-halide systems like $CsPb(Br/Cl)_3$ allow continuous spectral adjustment, vital for ratiometric sensing.[37,39] However, Pb^{2+} toxicity poses challenges, necessitating stringent handling and

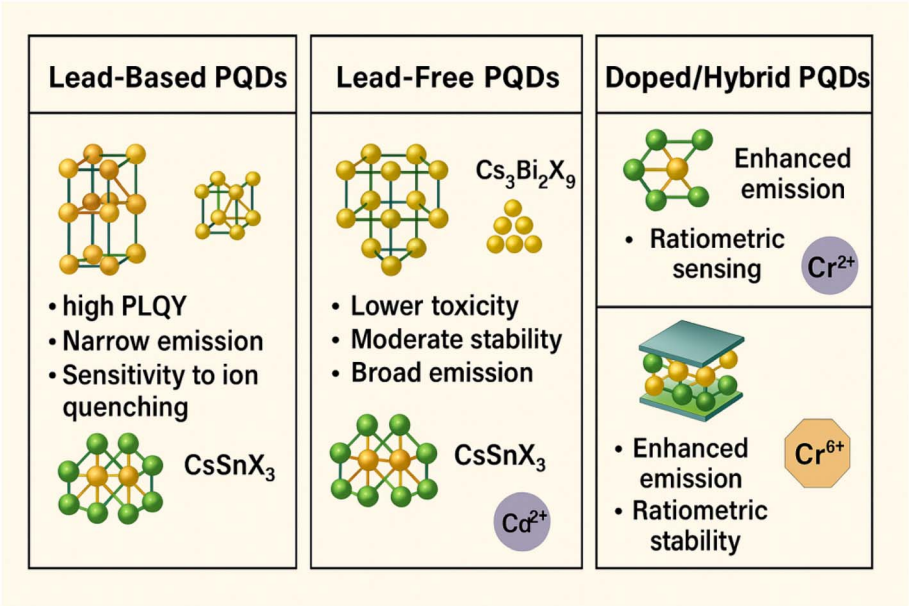

Fig. 3 Classification of PQDs into lead-based, lead-free, and doped/hybrid types, highlighting their structural features, optical properties, and sensing capabilities for heavy metal ion detection.

 © 2025 The Author(s). Published by the Royal Society of Chemistry

Open Access Article. Published on 23 October 2025. Downloaded on 10/25/2025 7:28:42 PM.
This article is licensed under a Creative Commons Attribution 3.0 Unported Licence.

disposal protocols for environmental and biological sensing applications.

2.2.2. Lead-free perovskite quantum dots. Lead-free PQDs, such as $Cs_3Bi_2X_9$, $CsSnX_3$, or $MASnX_3$, are developed to address the toxicity concerns of lead-based counterparts. These materials replace Pb^{2+} with less toxic metals like Bi^{3+} or Sn^{2+}. $Cs_3Bi_2X_9$ PQDs adopt a layered or dimer structure rather than the standard ABX_3 perovskite lattice, resulting in lower PLQY (typically 20–50%) and broader emission spectra (FWHM ~40–60 nm).[40] Despite these limitations, they offer improved environmental stability and are suitable for detecting ions like Cu^{2+} or Cr^{6+} in aqueous media. $CsSnX_3$ PQDs, while promising, suffer from rapid oxidation of Sn^{2+} to Sn^{4+}, leading to reduced stability and PL efficiency.[37] Doping strategies, such as incorporating Eu^{3+} or Mn^{2+}, enhance the optical properties and stability of lead-free PQDs, making them viable for eco-friendly sensing applications.

2.2.3. Doped and hybrid perovskite quantum dots. Doping PQDs with transition metal ions (*e.g.*, Mn^{2+}, Eu^{3+}) or forming hybrid structures (*e.g.*, $CsPbBr_3$–MXene) introduces additional functionalities. Mn^{2+}-doped $CsPbCl_3$ PQDs exhibit dual emission (excitonic and dopant-induced), enabling ratiometric sensing for improved accuracy. Hybrid structures, such as $CsPbBr_3$ encapsulated in metal–organic frameworks (MOFs) or combined with MXene, enhance stability and sensitivity by providing a protective matrix or facilitating charge transfer.[41] These advanced PQDs are particularly effective for detecting multiple analytes, including heavy metal ions, in complex matrices (Fig. 3).

2.2.4. Comparison of PQD types. The diverse classes of PQDs exhibit distinct optical, structural, and stability characteristics, making them suitable for various sensing applications. Lead-based PQDs offer superior PLQY and tunable emission but are hindered by toxicity and environmental concerns. In contrast, lead-free PQDs prioritize eco-friendliness and stability, albeit with compromised optical performance. Doped and hybrid PQDs combine enhanced stability and multifunctionality, enabling advanced sensing capabilities in complex environments. The below table summarizes their key properties to facilitate a comparative understanding (Table 1).

2.3. Synthesis methods and their impact on sensing performance

The synthesis strategy employed for PQDs plays a critical role in determining their particle size, crystallinity, surface chemistry, and ultimately their performance in sensing applications. Controlled synthesis influences the PLQY, surface defect density, ion accessibility, and stability in aqueous media—key parameters governing their suitability for detecting heavy metal ions. This section systematically discusses five major synthesis methods, highlighting their operational principles, advantages, and limitations, as well as their implications for sensor performance.

2.3.1. Hot-injection method. The hot-injection method is one of the most widely used and precise techniques for synthesizing high-quality PQDs. Typically, cesium oleate is

Table 1 Comparative overview of perovskite quantum dot types and their properties

PQD type	Composition example	Lead-based/lead-free	PLQY (%)	Emission range (nm)	Stability	Sensing applications	Ref.
Inorganic lead-based	$CsPbX_3$ (X = Cl, Br, I)	Lead-based	50–90	410–680	Moderate (sensitive to moisture/UV)	Cu^{2+}, Hg^{2+}, Cd^{2+} detection	37 and 39
Organic–inorganic hybrid	$CH_3NH_3PbX_3$, $FAPbX_3$	Lead-based	40–80	450–700	Low (volatile organic cations)	Cu^{2+}, Fe^{3+} detection	42
Lead-free bismuth-based	$Cs_3Bi_2X_9$	Lead-free	20–50	400–600	High (water-stable)	Cu^{2+}, Cr^{6+} detection	43
Lead-free tin-based	$CsSnX_3$, $MASnX_3$	Lead-free	10–40	600–800	Low (Sn^{2+} oxidation)	Pb^{2+} detection	44 and 45
Doped/hybrid	$CsPbCl_3$:Mn, $CsPbBr_3$@MOF	Lead-based/lead-free	30–80	400–700	High (matrix-protected)	Ratiometric sensing, multi-ion detection	41

Open Access Article. Published on 23 October 2025. Downloaded on 10/25/2025 7:28:42 PM.
This article is licensed under a Creative Commons Attribution 3.0 Unported Licence.

rapidly injected into a hot solution (140–200 °C) containing a lead halide precursor (*e.g.*, $PbBr_2$) dissolved in a non-coordinating solvent (*e.g.*, octadecene) along with ligands such as oleic acid (OA) and oleylamine (OAm), under an inert atmosphere (*e.g.*, N_2 or Ar). The sudden introduction of the cesium source induces burst nucleation followed by controlled growth, yielding monodisperse nanocrystals with tunable sizes (2–8 nm) and high crystallinity. This technique allows precise control over the halide composition (Cl^-, Br^-, I^-) and particle size, enabling direct tuning of bandgap and emission wavelength. PQDs synthesized by hot-injection typically exhibit PLQYs above 80% and low surface defect densities.[46,47] These features contribute to enhanced sensing performance through efficient fluorescence quenching mechanisms such as cation exchange or electron transfer, with LODs reaching sub-nanomolar levels for ions like Cu^{2+} and Hg^{2+}. However, the method requires rigorous control of reaction parameters and inert conditions, limiting scalability and water stability unless surface modification or encapsulation is performed.

2.3.2. Hydrothermal and solvothermal synthesis. Hydrothermal (aqueous-based) and solvothermal (organic solvent-based) methods involve sealing precursors in an autoclave and heating to elevated temperatures (100–200 °C) and pressures for several hours. These methods are particularly well-suited for the synthesis of lead-free PQDs, such as $Cs_3Bi_2X_9$ or $CsSnX_3$, offering improved environmental compatibility. The

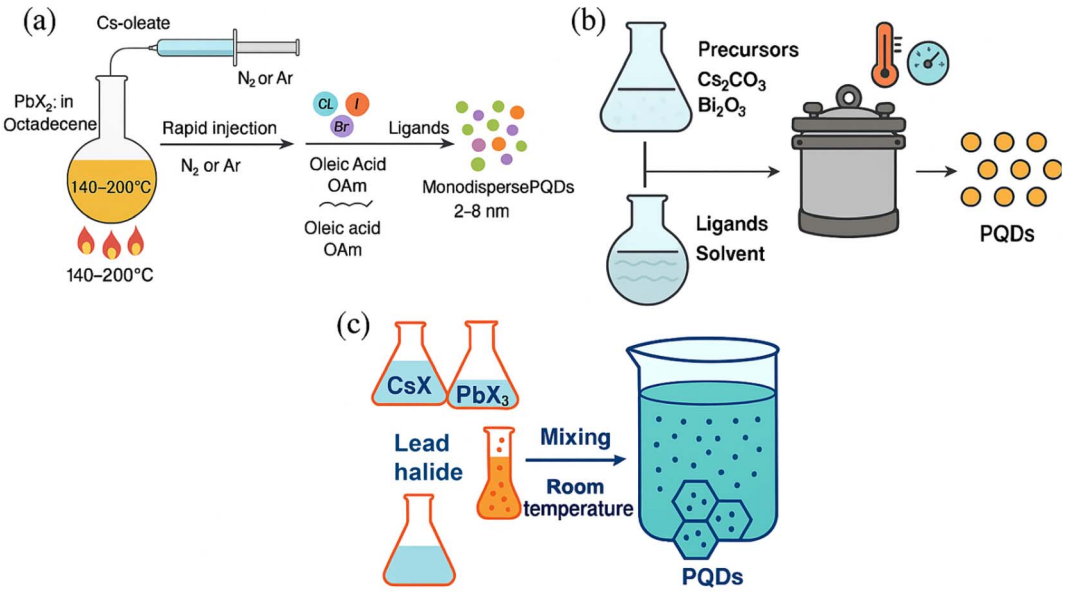

Fig. 4 Diverse synthetic routes for perovskite quantum dots: (a) hot-injection method; (b) hydrothermal and solvothermal synthesis procedures; (c) room-temperature precipitation technique.

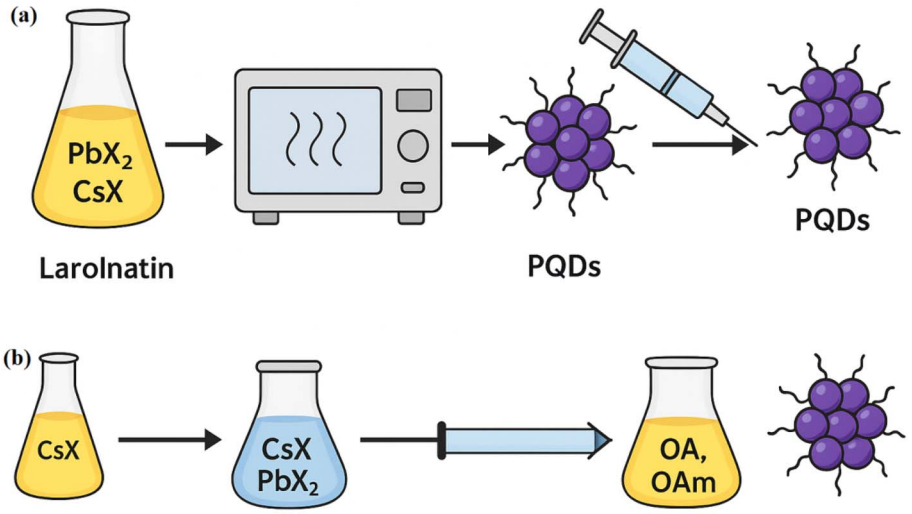

Fig. 5 Synthesis approaches for PQDs: (a) microwave-assisted synthesis technique; (b) ligand-assisted reprecipitation method.

 © 2025 The Author(s). Published by the Royal Society of Chemistry

Open Access Article. Published on 23 October 2025. Downloaded on 10/25/2025 7:28:42 PM.
This article is licensed under a Creative Commons Attribution 3.0 Unported Licence.

high-pressure environment promotes better ligand coordination, resulting in nanocrystals with moderate crystallinity and PLQYs in the range of 50–70%. Moreover, these methods yield PQDs with enhanced water stability, essential for applications in aqueous sensing.[48,49] Nevertheless, they often require longer reaction times and complex equipment setups, which can impede throughput and reproducibility.

2.3.3. Room-temperature precipitation. This method represents the most accessible and energy-efficient approach to PQD synthesis. It typically involves mixing cesium and lead halide salts in low-boiling point solvents such as ethanol or water under ambient conditions. While advantageous for rapid and low-cost production, this approach generally yields PQDs with larger sizes (8–15 nm), poor crystallinity, and high surface defect densities. These features reduce the PLQY (30–50%) and make the resulting nanocrystals less suitable for high-sensitivity detection. Nonetheless, this method finds utility in preliminary screening studies or applications where ultra-trace detection is not required.[50,51] It is particularly appealing in resource-limited settings where access to sophisticated equipment is restricted (Fig. 4).

2.3.4. Microwave-assisted synthesis. Microwave-assisted synthesis employs dielectric heating to rapidly and uniformly heat reaction mixtures, enabling accelerated nucleation and growth of PQDs. Typically, lead halide and cesium precursors are combined with coordinating ligands and subjected to microwave irradiation for short durations (minutes), resulting in highly crystalline PQDs with size ranges of 3–10 nm and PLQYs between 60–85%. The homogeneous temperature profile minimizes thermal gradients and suppresses defect formation, contributing to enhanced stability and sensitivity. Microwave synthesis is particularly effective for generating PQDs used in ratiometric sensing, such as dual-emission systems for Fe^{3+} and Cr^{6+} detection.[52,53] However, the method requires specialized microwave reactors and may present challenges in scaling for industrial use.

2.3.5. Ligand-assisted reprecipitation. LARP is a room-temperature, scalable approach ideal for cost-effective PQD production. In this method, precursors (*e.g.*, CsX and PbX_2) are dissolved in a polar solvent such as *N*,*N*-dimethylformamide (DMF) and rapidly injected into a non-polar solvent like toluene or hexane containing capping ligands (*e.g.*, OA, OAm). The difference in solubility induces supersaturation and instantaneous nucleation of PQDs. Although LARP-synthesized PQDs typically have broader size distributions (5–12 nm) and moderate PLQY (50–70%), the process is simpler and better suited for large-scale production. The nature and concentration of ligands significantly affect the colloidal stability, ion accessibility, and defect passivation.[54,55] By incorporating hydrophilic or zwitterionic ligands, water compatibility is improved, enabling application in aqueous sensing environments. However, LARP products often require post-synthetic treatments (*e.g.*, ligand exchange, encapsulation) to enhance long-term stability and minimize surface defects (Fig. 5).

Table 2 provides a comparative overview of commonly used PQD synthesis techniques, highlighting key physicochemical

Table 2 Comparison of synthesis methods for PQDs and their impact on heavy metal ion sensing performance

Synthesis method	Precursor type	Size (nm)	PLQY (%)	Defect density	Ion accessibility	Water compatibility	Scalability	Sensing performance	Ref.
Hot-injection	Cs-oleate + PbX_2 in OA/OAm	2–8	>80	Very low	Moderate–low	Low (requires treatment)	Low	High sensitivity (<1 nM); efficient quenching	46 and 47
Hydro/solvothermal	BiX_3 or SnX_2 + CsX in sealed autoclave	5–12	50–70	Moderate	Moderate	High	Medium	Moderate sensitivity (~tens of nM); lead-free options	48 and 49
Room-temp precipitation	PbX_2 + CsX in ethanol/water	8–15	30–50	High	High	High	Very high	Low sensitivity (>μM); fast and inexpensive	50 and 51
Microwave-assisted	Same as hot-injection	3–10	60–85	Low	Moderate	Moderate	Medium	High sensitivity (<5 nM); rapid synthesis	52 and 53
LARP	CsX + PbX_2 in DMF/toluene	5–12	50–70	Moderate	High (short ligands)	Moderate (hydrophilic ligands)	High	Moderate sensitivity; water-compatible	54 and 55

Open Access Article. Published on 23 October 2025. Downloaded on 10/25/2025 7:28:42 PM. This article is licensed under a Creative Commons Attribution 3.0 Unported Licence.

properties and their implications for heavy metal ion detection sensitivity and stability.

3. Mechanisms of heavy metal ion detection

The detection of heavy metal ions using PQDs leverages their unique optoelectronic properties, including high PLQY, narrow emission spectra, and tunable bandgaps, to achieve sensitive and selective responses to analyte interactions. These responses primarily manifest as changes in PL intensity, such as quenching or, less commonly, enhancement, driven by specific physical and chemical interactions between PQDs and metal ions.[56–58] This section explores the fundamental mechanisms underlying these interactions, including cation exchange, electron transfer, FRET, surface trap-mediated quenching, and charge transfer complex formation. The critical role of surface ligands in modulating selectivity and sensitivity is also discussed, alongside theoretical insights from computational methods, such as density functional theory (DFT) and molecular dynamics (MD) simulations, to elucidate the electronic and structural factors governing these mechanisms. The focus is on the fundamental processes, avoiding overlap with sensor performance or applications, which are reserved for subsequent sections.

3.1. Fluorescence quenching and enhancement mechanisms

The interaction of heavy metal ions with PQDs typically results in fluorescence quenching, where PL intensity decreases due to the creation of non-radiative recombination pathways, or, in rare cases, enhancement, where PL intensity increases due to passivation of surface defects. These changes stem from alterations in the electronic structure, surface chemistry, or energy transfer dynamics of PQDs, driven by distinct mechanisms.[11,59]

3.1.1. Cation exchange. Cation exchange is a dominant mechanism in lead-based PQDs, such as $CsPbX_3$ (X = Cl, Br, I) or $CH_3NH_3PbX_3$, where heavy metal ions replace the B-site cation (typically Pb^{2+}) at the PQD surface. This substitution disrupts the perovskite lattice, introducing defects or mid-gap states that facilitate non-radiative recombination, leading to fluorescence quenching. For example, Hg^{2+} ions, with an ionic radius (110 pm) close to Pb^{2+} (119 pm), readily replace Pb^{2+} in $CH_3NH_3PbBr_3$, causing lattice strain and quenching PL within seconds due to rapid ion exchange kinetics.[59] The selectivity of this mechanism depends on the ionic radius, charge, and coordination chemistry of the analyte, making it highly effective for Hg^{2+} detection over other ions like Zn^{2+} or Na^{+}. In lead-free PQDs, such as $Cs_3Bi_2X_9$, cation exchange is less prevalent due to the higher stability of Bi^{3+}, limiting this mechanism's applicability.[60] The efficiency of cation exchange is also influenced by surface ligand density, which can either facilitate or hinder ion access to the lattice.[61]

Panel (a) in Fig. 6 presents a TEM image of $CH_3NH_3PbBr_3$ QDs, revealing their nanoscale dimensions and uniform distribution, with a scale bar of 50 nm, consistent with the 2–10 nm range where quantum confinement effects dominate.[59] Panel (b) shows the size distribution analysis, indicating an average diameter of 5.3 ± 0.5 nm, which influences the discrete energy levels and size-dependent bandgap, enhancing photoluminescence properties critical for sensing applications. These structural characteristics support the cation exchange mechanism, where the surface accessibility of Pb^{2+} (ionic radius 119 pm) facilitates rapid ion substitution by analytes like Hg^{2+} (110 pm), disrupting the lattice and introducing defects. Panel (c) displays UV-vis absorption and photoluminescence emission spectra of $CH_3NH_3PbBr_3$ QDs, with an absorption edge around 520 nm and a sharp emission peak at 510 nm, reflecting the high oscillator strength and narrow FWHM (12–40 nm) due to quantum confinement. The inset photograph confirms the green emission, which is quenched upon Hg^{2+} exchange due to non-radiative recombination induced by lattice strain. Panel (d) presents XRD patterns of $CH_3NH_3PbBr_3$ QDs in the absence and presence of Hg^{2+}, showing peak shifts that indicate lattice disruption and mid-gap states formation, highlighting the selectivity and rapid kinetics of cation exchange for Hg^{2+} detection over other ions. Panel (e) illustrates the evolution of fluorescence spectra of $CH_3NH_3PbBr_3$ QDs with increasing Hg^{2+} concentrations (0 to 1000 nM), showing a progressive quenching of the 510 nm emission peak, consistent with cation exchange disrupting the perovskite lattice and enhancing non-radiative recombination. Panel (f) provides a linear fitting curve of I_0/I *versus* Hg^{2+} concentration (0–100 nM), with a correlation coefficient ($R^2 = 0.994$), demonstrating the sensitivity and selectivity of this mechanism for Hg^{2+} detection, influenced by ionic radius compatibility and surface ligand density that modulates ion access.

3.1.2. Electron transfer. Electron transfer occurs when heavy metal ions interact with the PQD surface, enabling the transfer of electrons from the conduction band of the PQD to the ion's unoccupied orbitals or *vice versa*, creating non-radiative recombination pathways that quench fluorescence. For instance, Cu^{2+} ions, with their partially filled d-orbitals, act as electron acceptors in $CsPbBr_3$ PQDs, reducing PL intensity by accepting electrons from the conduction band.[62] This mechanism is particularly effective for transition metal ions like Cu^{2+}, Fe^{3+}, or Cr^{6+}, whose redox potentials align with the PQD's band structure, facilitating efficient electron transfer.[62,63] The quenching efficiency depends on the energy level alignment between the PQD's conduction band and the ion's orbitals, as well as the accessibility of the PQD surface, which is modulated by ligands. Electron transfer is more pronounced in organic solvents, where ligands like OAm allow ion access, but may be limited in aqueous media due to ligand barriers.[61]

3.1.3. Förster resonance energy transfer. FRET involves non-radiative energy transfer from the excited state of a PQD (donor) to a heavy metal ion or a nearby acceptor molecule, resulting in fluorescence quenching. FRET requires spectral overlap between the PQD's emission and the acceptor's absorption spectrum, as well as proximity within 10 nm. For example, in a ratiometric sensor, $CsPbBr_3$ PQDs transfer energy to gold nanoclusters in the presence of Cu^{2+}, quenching the PQD's green emission (~520 nm) while enhancing the

 © 2025 The Author(s). Published by the Royal Society of Chemistry

Open Access Article. Published on 23 October 2025. Downloaded on 10/25/2025 7:28:42 PM.
This article is licensed under a Creative Commons Attribution 3.0 Unported Licence.

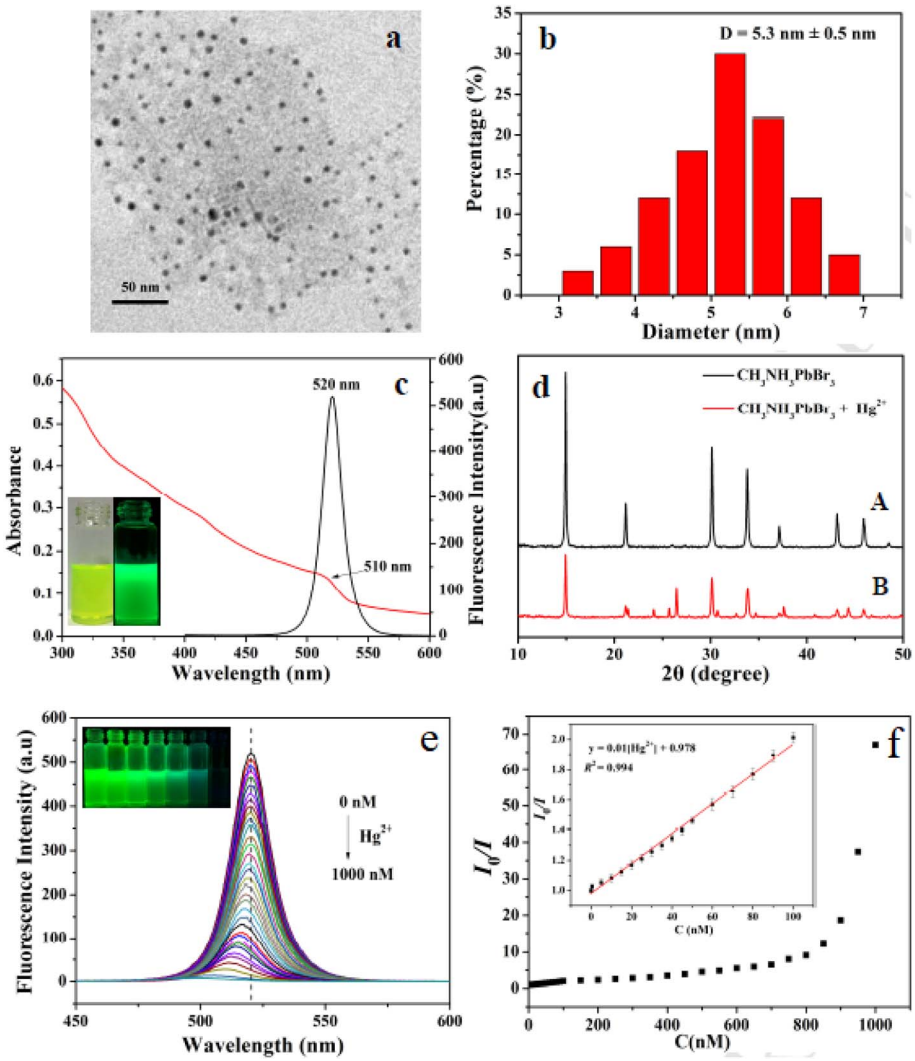

Fig. 6 (a) TEM image of $CH_3NH_3PbBr_3$ QDs, (b) size distribution of $CH_3NH_3PbBr_3$ QDs, (c) UV-vis and PL spectra of $CH_3NH_3PbBr_3$ QDs, (d) XRD patterns with/without Hg^{2+}, (e) fluorescence changes with varying Hg^{2+}, (f) I_0/I *vs.* Hg^{2+} (0–100 nM) linear fit. Reprinted with permission from ref. 59. Copyright 2017, Elsevier.

nanocluster's emission due to spectral overlap.[64] FRET is highly sensitive but less selective, as multiple analytes may induce similar energy transfer effects, necessitating careful sensor design to ensure specificity.[65] The efficiency of FRET depends on the dipole–dipole coupling strength, which is influenced by the PQD's emission properties and the ligand-mediated distance between the PQD and the acceptor.[66]

3.1.4. Surface trap-mediated quenching. Surface trap-mediated quenching occurs when heavy metal ions interact with surface defects or trap states on PQDs, such as uncoordinated halide ions or underpassivated cation sites, creating non-radiative recombination centers that quench fluorescence. For instance, Fe^{3+} ions bind to surface defects on $CsPbBr_3$–$CsPb_2Br_5$ PQDs, forming trap states that capture excitons and reduce PL intensity.[67] This mechanism is particularly relevant for PQDs with high surface-to-volume ratios, where defects are more prevalent. In lead-free PQDs like $MASnBr_3$, surface trap-mediated quenching is enhanced by the interaction of ions like Cr^{6+} with undercoordinated Sn^{2+} sites, leading to efficient quenching.[68] The extent of quenching depends on the defect density and ligand passivation, which can either suppress or amplify trap-mediated effects. Surface modification with ligands like APTES can reduce defect density, mitigating non-specific quenching and enhancing selectivity.[67]

3.1.5. Charge transfer complex formation. Charge transfer complex formation involves the creation of a transient complex between the PQD surface and a heavy metal ion, leading to fluorescence quenching through the formation of a charge transfer state. This mechanism is driven by the coordination of metal ions with surface ligands or lattice ions, forming a complex that alters the electronic structure of the PQD. For example, Cu^{2+} ions can form coordination complexes with amine groups on $CsPbBr_3$ PQDs, creating a charge transfer state that quenches PL by redirecting excitons to non-radiative pathways.[69] This mechanism is particularly effective for ions with strong coordination abilities, such as Cu^{2+} or Cd^{2+}, and is

Open Access Article. Published on 23 October 2025. Downloaded on 10/25/2025 7:28:42 PM.
This article is licensed under a Creative Commons Attribution 3.0 Unported Licence.

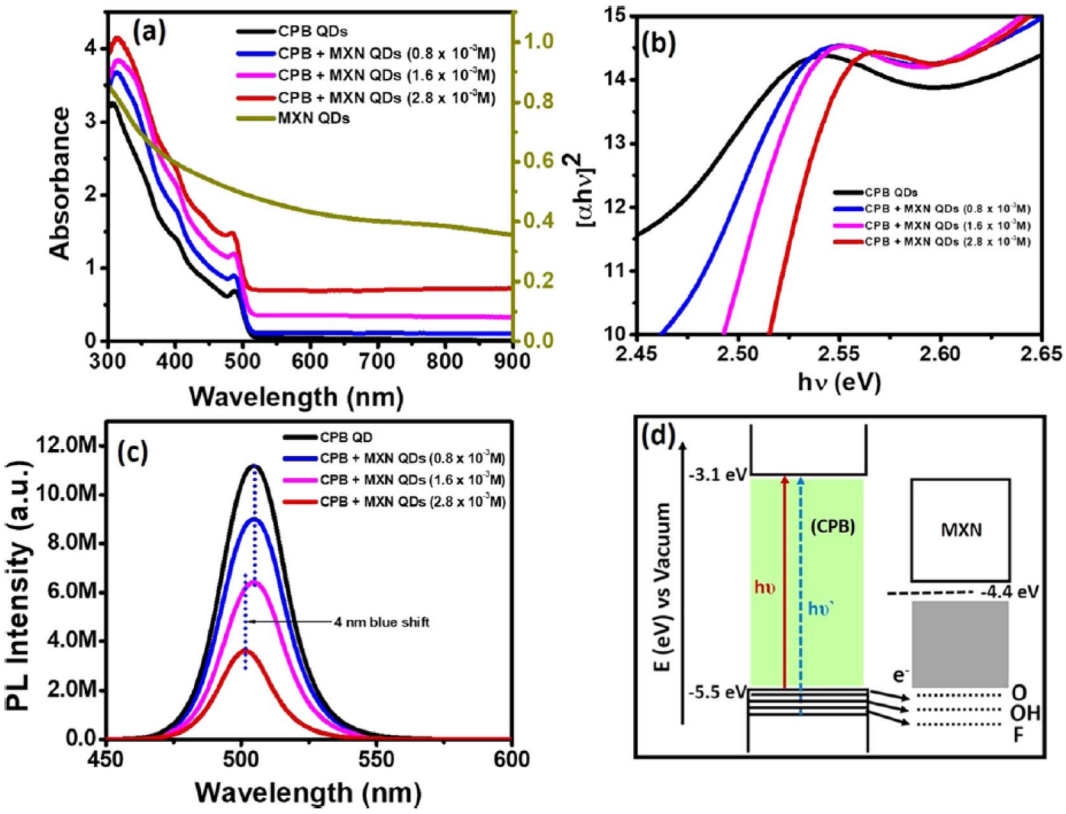

Fig. 7 (a) Absorbance spectra of $CsPbBr_3$ QDs, MXN QDs, and CPB-MXN composites, (b) Tau plots of CPB-MXN *vs.* pure $CsPbBr_3$, (c) PL spectra of CPB-MXN with MXN concentrations 0.8×10^{-3}, 1.6×10^{-3}, 2.8×10^{-3} M, (d) schematic of CPB-MXN band alignment. CPB QD concentration is constant (1.9×10^{-7} M). Reprinted with permission from ref. 70. Copyright 2020, American Chemical Society.

enhanced in heterostructures like $CsPbBr_3$–$Ti_3C_2T_x$ MXene, where the MXene facilitates charge transfer.[70] The stability and quenching efficiency of the complex depend on the ligand's coordination strength and the ion's electronegativity.

Panel (a) in Fig. 7 presents absorbance spectra of $CsPbBr_3$ QDs (black line), MXN QDs (dark yellow), and $CsPbBr_3$ QD–$Ti_3C_2T_x$ QD (CPB-MXN) composites, showing distinct absorption edges influenced by the formation of charge transfer complexes, where heavy metal ions coordinate with surface ligands, altering the electronic structure [ref. 70]. Panel (b) in Fig. 7 displays tau plots of the CPB-MXN composite compared to pure $CsPbBr_3$, indicating faster decay rates due to charge transfer states that redirect excitons to non-radiative pathways. Panel (c) shows steady-state PL spectra at 410 nm excitation for the CPB-MXN composite with varying MXN concentrations (0.8×10^{-3}, 1.6×10^{-3}, 2.8×10^{-3} M), revealing a 4 nm blue shift and quenching, consistent with the transient complex formation that enhances non-radiative recombination, particularly with ions like Cu^{2+} coordinating with amine groups. Panel (d) provides a schematic diagram of the CPB-MXN band alignment, illustrating the energy levels where the charge transfer state forms, with a vacuum level at −3.1 eV and a bandgap of 2.4 eV for CPB, facilitating efficient charge transfer in heterostructures like $CsPbBr_3$–$Ti_3C_2T_x$ MXene. This alignment supports the quenching mechanism driven by strong coordination abilities of ions such as Cu^{2+} or Cd^{2+}, enhanced by the MXene's role in facilitating charge transfer. The stability and efficiency of this quenching depend on the ligand's coordination strength and the ion's electronegativity, aligning with the mechanism's effectiveness in altering the PQD's electronic structure for sensing applications.

3.2. Role of surface ligands in selectivity and sensitivity

Surface ligands, such as OAm, OA, PEI, hydroxypropyl chitosan, or APTES, are critical in modulating the selectivity and sensitivity of PQD-based detection. Ligands passivate surface defects, stabilize colloidal dispersions, and mediate ion–PQD interactions, influencing the efficiency of quenching or enhancement mechanisms. Long-chain ligands like OAm and OA provide steric hindrance, reducing non-specific interactions and enhancing selectivity for ions like Hg^{2+} or Cu^{2+}, which penetrate the ligand shell through coordination or ion exchange.[61] For example, OAm-capped $CsPbBr_3$ PQDs exhibit high selectivity for Cu^{2+} due to the ion's ability to coordinate with amine groups, facilitating electron transfer or complex formation.[62] However, dense ligand layers may reduce sensitivity by limiting ion access, particularly in aqueous media. Hydrophilic or zwitterionic ligands, such as hydroxypropyl chitosan, improve water compatibility and ion accessibility, enhancing sensitivity for ions like Cr^{6+}.[71] PEI-modified $MASnBr_3$ PQDs introduce chelating groups that selectively bind Fe^{3+}, forming stable complexes that enhance quenching specificity.[68]

 © 2025 The Author(s). Published by the Royal Society of Chemistry

Open Access Article. Published on 23 October 2025. Downloaded on 10/25/2025 7:28:42 PM. This article is licensed under a Creative Commons Attribution 3.0 Unported Licence.

Dynamic ligand exchange, where metal ions displace weakly bound ligands, exposes the PQD surface, amplifying quenching through cation exchange or trap-mediated mechanisms. For instance, Cd^{2+} detection with $CsPbBr_3$–$CsPb_2Br_5$ PQDs is enhanced by ammonia hydroxide, which reduces ligand density and increases surface accessibility.[72] Conversely, strongly bound ligands like APTES improve stability and selectivity for Fe^{3+} by minimizing non-specific interactions.[67]

3.3. Theoretical insights

Theoretical studies, particularly DFT calculations using functionals like PBE or HSE06 for accurate band structures, provide quantitative insights into the electronic, structural, and kinetic changes induced by heavy metal ions in PQDs. For cation exchange, DFT simulations of Pb^{2+} substitution with Hg^{2+} in $CH_3NH_3PbBr_3$ reveal the formation of mid-gap states positioned 0.5–1.0 eV below the conduction band (CB, typically at −3.5 eV *vs.* vacuum), which promote non-radiative recombination by increasing the rate constant from $\sim 10^7$ s^{-1} (pristine) to $\sim 10^9$ s^{-1}, as evidenced by shortened PL lifetimes from 10 ns to ~2 ns.[59] The thermodynamic rationale is rooted in a favorable Gibbs free energy change ($\Delta G \approx -20$ to -25 kJ mol^{-1}), calculated from the low lattice distortion energy due to similar ionic radii (Pb^{2+}: 119 pm; Hg^{2+}: 110 pm) and a reduced activation barrier (~0.2 eV), enabling rapid exchange kinetics on the order of seconds in organic solvents. This mechanism is particularly selective for Hg^{2+}, with ΔG more negative than for mismatched ions like Zn^{2+} ($\Delta G > -10$ kJ mol^{-1}), aligning with experimental quenching efficiencies >90%.[59]

Similarly, for electron transfer, Cu^{2+} binding to $CsPbBr_3$ surfaces reduces the bandgap by shifting the CB edge downward by 0.3–0.4 eV (from −3.8 eV to −4.1 eV), facilitating efficient electron donation from the PQD CB to Cu^{2+} unoccupied d-orbitals (LUMO at ~−4.0 eV), with transfer rates $\sim 5 \times 10^{10}$ s^{-1}—significantly faster than other mechanisms like FRET ($\sim 10^8$ s^{-1}).[62] Thermodynamically, this is driven by a $\Delta G \approx -15$ to -18 kJ mol^{-1}, arising from redox potential alignment (Cu^{2+}/Cu^+ $E^\circ = 0.15$ V *vs.* NHE, matching PQD CB at ~−0.5 V), which lowers the energy barrier for charge separation and enhances quenching in transition metal detections. In lead-free $Cs_3Bi_2Br_9$, DFT indicates Cu^{2+} interactions with Bi^{3+} sites create shallow trap states at 0.2–0.3 eV above the valence band (VB at −5.5 eV), increasing non-radiative rates to $\sim 8 \times 10^8$ s^{-1} with a $\Delta G \approx -12$ to -14 kJ mol^{-1}, though kinetics are slower due to higher lattice rigidity (activation energy ~0.4 eV) compared to lead-based systems.[60] This highlights a trade-off: lead-free PQDs offer eco-friendly thermodynamics but reduced kinetic efficiency for aqueous sensing.

Bandgap effects are central to all detection mechanisms, where metal ions shift band edges and alter recombination pathways. For surface trap-mediated quenching, Fe^{3+} ions induce a redshift in the bandgap of $CsPbBr_3$–$CsPb_2Br_5$ by 0.15–0.2 eV (from 2.4 eV to 2.2 eV), driven by strong electrostatic binding (energy ~ −1.5 to −2.0 eV), which creates defect states and reduces radiative lifetimes from 10–15 ns to 1–3 ns, corresponding to rate increases to 6×10^8 s^{-1}.[67] Thermodynamically, $\Delta G \approx -19$ kJ mol^{-1} favors trap formation due to Fe^{3+} coordination with underpassivated Br^- sites, making this mechanism kinetically slower than electron transfer but highly selective in aqueous matrices with pH-dependent interferences. DFT also elucidates ligand roles, showing that ligand–metal coordination (*e.g.*, OAm or PEI with Cu^{2+}) lowers electron transfer barriers by 0.3–0.5 eV, increasing rates by 10–100-fold and ΔG by −5 to −10 kJ mol^{-1} through stabilized charge-separated states.[73] This is particularly relevant for ratiometric designs, where FRET efficiencies reach 60–70% with dipole–dipole distances < 10 nm, but kinetics lag ($\sim 10^8$ s^{-1}) due to spectral overlap requirements (>50% emission–absorption match) and less negative ΔG (~−10 kJ mol^{-1}) compared to direct transfer.

MD simulations further model ion kinetics, revealing that diffusion through the ligand shell (*e.g.*, oleylamine chains ~ 1–2 nm thick) is rate-limiting, with diffusion coefficients $\sim 5 \times 10^{-10}$ to 10^{-9} m^2 s^{-1} and residence times ~10–100 ps, affecting overall response times (seconds in experiments).[74] Comparatively, electron transfer exhibits the fastest kinetics (10^{10} s^{-1}, low barriers) and most negative ΔG for rapid, sensitive detection of transition metals like Cu^{2+}; cation exchange offers intermediate rates (10^9 s^{-1}) with high thermodynamic stability for Hg^{2+}-specific sensing; while trap-mediated and FRET mechanisms provide tunable selectivity but slower dynamics (10^8 s^{-1}) due to defect/spectral dependencies. These quantitative metrics, validated by hybrid DFT-MD approaches, guide rational PQD design—*e.g.*, ligand engineering to optimize barriers or doping to align band edges—for enhanced sensitivity (sub-nM LODs) and selectivity in diverse matrices.

4. PQD-based nanosensors for heavy metal ion detection

PQDs have emerged as highly effective platforms for detecting heavy metal ions, leveraging their exceptional optoelectronic properties, including high PLQY, tunable emission wavelengths, and large surface-to-volume ratios. These attributes enable the development of sensors with superior sensitivity and selectivity, particularly for industrial applications where precise detection of heavy metal contaminants is critical.[11,38] This section reviews the design of PQD-based nanosensors for specific heavy metal ions, evaluates their performance metrics, compares lead-based and lead-free PQDs, explores strategies for enhancing sensor performance, and details their applications in industrial settings for heavy metal detection. The focus is on practical sensor design and performance, distinct from the mechanistic insights covered previously, ensuring a comprehensive and application-oriented analysis tailored to the detection of heavy metal ions.

4.1. Design of PQD-based nanosensors for specific heavy metal ions

The design of PQD-based nanosensors is tailored to detect specific heavy metal ions, including Hg^{2+}, Cu^{2+}, Cd^{2+}, Fe^{3+}, Cr^{6+}, and Pb^{2+}, by exploiting ion-specific interactions with the PQD surface or lattice. For Hg^{2+} detection, $CH_3NH_3PbBr_3$ PQDs have

Open Access Article. Published on 23 October 2025. Downloaded on 10/25/2025 7:28:42 PM.
This article is licensed under a Creative Commons Attribution 3.0 Unported Licence.

been developed with a limit of detection (LOD) of 0.124 nM, capitalizing on their high PLQY (50.28%) and efficient surface interactions that lead to fluorescence quenching.[59] The sensor design leverages the chemical affinity of Hg^{2+} for the perovskite lattice, enabling rapid and selective detection in organic media. Cu^{2+} detection is a focal point, with $CsPbBr_3$ PQDs achieving an LOD of 0.1 nM in organic solvents like hexane, benefiting from fast response times (<10 s) and high selectivity over competing ions such as Na^+ or Zn^{2+}.[62] The design incorporates ligands like OAm to facilitate ion access in non-polar environments. Cd^{2+} detection is achieved using $CsPbBr_3$–$CsPb_2Br_5$ PQDs modified with ammonia hydroxide, which reduces ligand density to enhance surface accessibility, resulting in an LOD of 10^{-6} M.[72] This modification improves sensitivity in aqueous media, critical for industrial wastewater analysis. Lead-free PQDs, such as $MASnBr_3$, are designed for Fe^{3+} and Cr^{6+} detection, achieving nanomolar sensitivity through tailored ligand systems like PEI, which forms selective complexes with these ions.[68] $Cs_3Bi_2Br_9$ PQDs are engineered for Cu^{2+} detection in aqueous environments, achieving an LOD of 98.3 nM due to their high photostability and ligand-assisted interactions.[60] For Pb^{2+} detection, $CsSnX_3$ PQDs are optimized for non-aqueous media like lubricants, achieving an LOD of 3.5 nM through synthesis methods that enhance PL stability.[75] These designs highlight the adaptability of PQDs to diverse ions and matrices, driven by tailored material compositions and surface chemistries.

Fig. 8a shows the PL intensity of $Cs_3Bi_2Br_9$ PQDs at varying Cu^{2+} concentrations (0 to 1200 nM), with a clear quenching trend, reflecting the high PLQY (50.28%) and efficient surface interactions that enable a low LOD of 0.1 nM in organic solvents like hexane, as designed for Cu^{2+} detection. Panel (b) presents a fitting curve for PL intensity *versus* Cu^{2+} concentration, demonstrating a linear range of 0–1200 nM with an R^2 of 0.99105, highlighting the sensor's selectivity and rapid response (<10 s) over competing ions like Na^+ or Zn^{2+}, facilitated by ligands such as OAm. Panel (c) displays time-resolved fluorescence spectra at varying Cu^{2+} concentrations, showing decay time reductions that underscore the fast ion-specific interactions with the PQD lattice, aligning with the tailored design for heavy metal ion sensing. Panel (d) illustrates the PL responses (F_0/F) of the probe to different metal ions (Zn^{2+}, Mg^{2+}, Sn^{2+}, Mn^{2+}, Ni^{2+}, Pb^{2+}, In^{3+}, Cu^{2+}), with Cu^{2+} exhibiting the highest quenching efficiency ($F_0/F \approx 3.5$), confirming the sensor's selectivity and nanomolar sensitivity (LOD 0.1 nM) for Cu^{2+} in organic media. This design leverages the chemical affinity of Cu^{2+} for the perovskite surface, enhanced by ligand-assisted interactions, consistent with the adaptability of PQDs like $Cs_3Bi_2Br_9$ for aqueous detection (LOD 98.3 nM) or $CH_3NH_3PbBr_3$

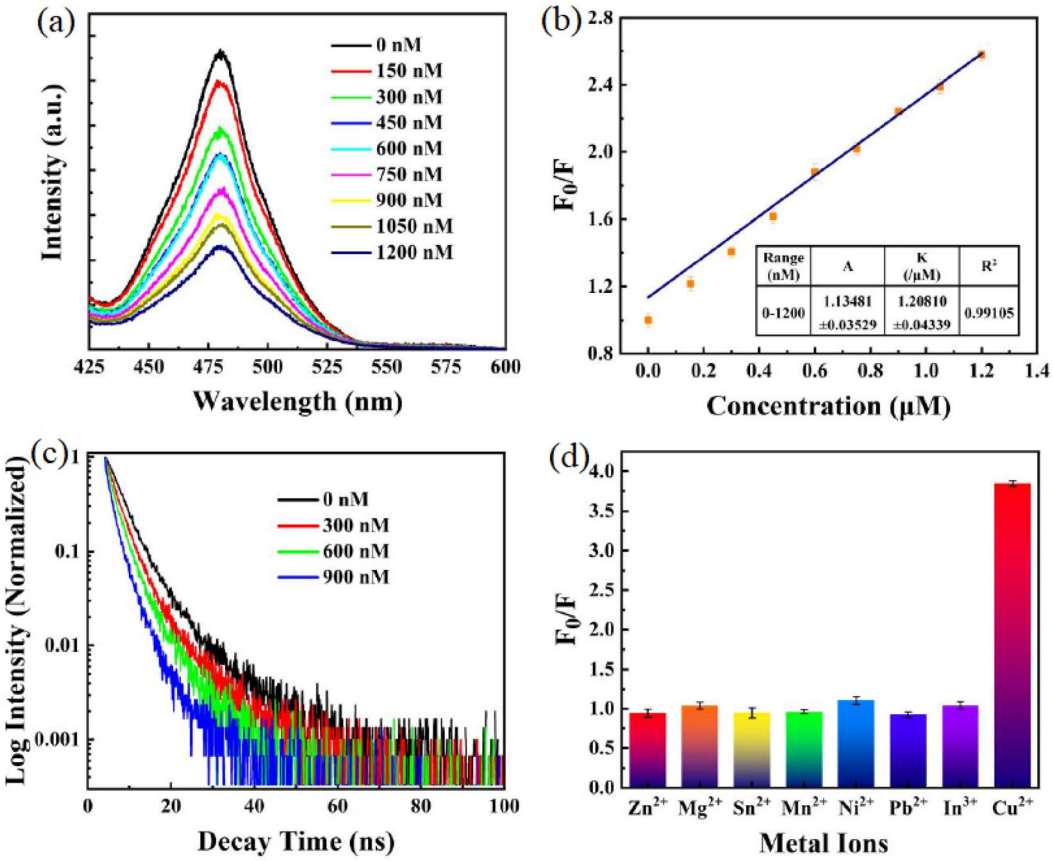

Fig. 8 (a) PL intensity of $Cs_3Bi_2Br_9$ PQDs at different Cu^{2+} concentrations, (b) calibration curve of PL intensity *versus* Cu^{2+} concentration, (c) time-resolved fluorescence profiles with varying Cu^{2+} levels, (d) PL responses of the sensor to various metal ions. Adapted with permission from ref. 60. Copyright 2023, MDPI.

 © 2025 The Author(s). Published by the Royal Society of Chemistry

Open Access Article. Published on 23 October 2025. Downloaded on 10/25/2025 7:28:42 PM.
This article is licensed under a Creative Commons Attribution 3.0 Unported Licence.

for Hg^{2+} (LOD 0.124 nM), and $CsSnX_3$ for Pb^{2+} (LOD 3.5 nM) in non-aqueous matrices, showcasing tailored surface chemistries for diverse ion-specific applications.

4.2. Performance metrics of PQD-based sensors

The performance of PQD-based nanosensors is evaluated through key metrics: sensitivity, selectivity, LOD, and linear detection range, all of which are critical for their practical application in industrial and environmental settings. These metrics are heavily influenced by the matrix in which detection occurs (*e.g.*, organic solvents like hexane, aqueous solutions, or complex media like seawater and wastewater), necessitating standardized calibration protocols, blank measurements, and interference assessments to ensure reproducibility and comparability.

Sensitivity is defined as the change in PL intensity per unit analyte concentration ($\Delta I/\Delta C$, typically in a.u./nM). Lead-based PQDs, such as $CsPbX_3$ (X = Cl, Br, I), exhibit high sensitivity due to their strong fluorescence (PL quantum yield, PLQY, 50–90%) and large absorption coefficients (10^5 to 10^6 cm^{-1}). For instance, $CsPbBr_3$ PQDs detect Cu^{2+} in hexane with a sensitivity of $\sim 10^3$ a.u./nM across a linear range of 0–1200 nM, calibrated using Stern–Volmer plots (I_0/I *vs.* $[Cu^{2+}]$) with blank hexane solutions to correct for background fluorescence.[62] In aqueous matrices, sensitivity often decreases due to matrix effects; for example, $Cs_3Bi_2Br_9$ in seawater shows a sensitivity of $\sim 10^2$ a.u./nM for Cu^{2+}, attributed to ionic strength (*e.g.*, 0.6 M NaCl) and pH variations (pH 7.5–8.5), requiring calibration with seawater blanks.[60]

Selectivity is achieved through specific interactions between PQDs and target ions, such as cation exchange for Hg^{2+} or chelation for Fe^{3+}, minimizing interference from common ions like K^+, Na^+, or Ca^{2+}. For example, $CH_3NH_3PbBr_3$ PQDs selectively detect Hg^{2+} in organic solvents with >95% selectivity over Zn^{2+} and Mg^{2+}, confirmed through interference tests where competing ions caused <5% PL change.[59] In complex matrices like wastewater (pH $\sim$ 6.5, high Ca^{2+}/Mg^{2+}), selectivity may drop to $\sim$80% unless ligand modifications (*e.g.*, polyethylenimine, PEI) enhance ion-specific binding.[68] Calibration protocols incorporate blank measurements in the respective matrix to establish baseline PL and interference tests to quantify selectivity (*e.g.*, PL quenching <10% for non-target ions).

LOD varies significantly with matrix and calibration methodology. In organic solvents like hexane, where ionic interferences are minimal, LODs reach sub-nanomolar levels (*e.g.*, 0.1 nM for Cu^{2+} with $CsPbBr_3$, determined *via* Stern–Volmer with 3σ/slope, where σ is the standard deviation of blank hexane fluorescence[62]). In contrast, aqueous matrices like seawater or wastewater yield higher LODs (*e.g.*, 98.3 nM for Cu^{2+} with $Cs_3Bi_2Br_9$ in seawater, calibrated *via* linear I_0/I fitting with seawater blanks and interference tests showing $\sim$15% quenching from Ca^{2+}/Mg^{2+} (ref. 60)). Complex matrices introduce challenges like ionic strength, pH fluctuations, and organic matter, which elevate LODs; for instance, wastewater (COD $\sim$ 200 mg L^{-1}) increases LODs to $\sim$500 nM for Fe^{3+} with $MASnBr_3$ due to competing quenching.[68] Ratiometric sensors, such as $CsPbBr_3$

Table 3 Summary of LODs and performance metrics for PQD-based sensors

PQD type	Ion	LOD	Matrix	Calibration protocol	Blanks/interferences	Selectivity	Linear range	Ref.
$CsPbBr_3$	Cu^{2+}	0.1 nM	Hexane	Stern–Volmer (3σ/slope)	Hexane blanks; <5% quenching by Na^+, Zn^{2+}	>95%	0–1200 nM	62
$Cs_3Bi_2Br_9$	Cu^{2+}	98.3 nM	Seawater	Linear I_0/I fitting	Seawater blanks; $\sim$15% quenching by Ca^{2+}, Mg^{2+} (ligand-mitigated)	$\sim$80%	0–1000 nM	60
$CH_3NH_3PbBr_3$	Hg^{2+}	0.124 nM	Organic solvent	I_0/I *vs.* concentration (3σ/slope)	Solvent blanks; <5% quenching by Zn^{2+}, Mg^{2+}	>95%	0–1000 nM	59
$MASnBr_3$	Fe^{3+}	$\sim$1 nM	Aqueous	Time-resolved decay (3σ/slope)	Water blanks; $\sim$10% quenching by Cr^{6+} (PEI-selective)	$\sim$90%	10^{-9} to 10^{-5} M	68
$CsPbBr_3$@MOF	Cu^{2+}	1.63 nM	Hexane	Fluorescence quenching plot	Hexane blanks; <8% quenching by K^+, Ca^{2+}	>92%	10^{-9} to 10^{-6} M	78
$CsPbBr_3$–$CsPb_2Br_5$	Cd^{2+}	1 μM	Wastewater	Stern–Volmer (3σ/slope)	Wastewater blanks; $\sim$20% quenching by Cu^{2+} (ligand-modified)	$\sim$75%	10–500 nM	72

Open Access Article. Published on 23 October 2025. Downloaded on 10/25/2025 7:28:42 PM. This article is licensed under a Creative Commons Attribution 3.0 Unported Licence.

paired with Au nanoclusters, mitigate matrix effects by using dual-emission ratios, achieving LODs of ~1 nM for Cu^{2+} in aqueous systems with calibration against blank water and <10% interference from Na^+/K^+.[64]

Linear detection range typically spans 10^{-9} to 10^{-3} M, depending on the matrix and PQD type. In organic solvents, $CsPbBr_3$ detects Cu^{2+} linearly from 0–1200 nM, with high R^2 (>0.99) in Stern–Volmer plots.[62] In seawater, $Cs_3Bi_2Br_9$ maintains linearity from 0–1000 nM but requires ligand passivation to counter matrix interferences.[60] Wastewater matrices narrow the range (*e.g.*, 10–500 nM for Fe^{3+} with $MASnBr_3$) due to pH and organic matter effects, calibrated *via* time-resolved decay to isolate analyte-specific quenching.[68]

To standardize comparisons across studies, Table 3 summarizes LODs, matrices, calibration protocols, blank measurements, interference tests, selectivity metrics, and linear ranges. Organic solvents generally yield lower LODs and wider ranges due to reduced interferences, while aqueous and complex matrices require robust calibration (*e.g.*, matrix-matched blanks) and ligand strategies to maintain performance. These insights guide sensor optimization for specific applications, such as trace metal detection in environmental monitoring.

4.3. Comparison of lead-based and lead-free PQDs for heavy metal ion detection

Lead-based PQDs, such as $CsPbX_3$ (X = Cl, Br, I) and $CH_3NH_3PbX_3$, are highly effective for detecting heavy metal ions due to their superior optoelectronic properties, including high photoluminescence quantum yield and narrow emission spectra. These attributes enable ultra-low LODs, often below 10 nM, for ions like Hg^{2+} and Cu^{2+}. For instance, $CH_3NH_3PbBr_3$ PQDs achieve an LOD of 0.124 nM for Hg^{2+}, with rapid response times (<10 s) and high sensitivity, making them suitable for environmental monitoring.[59] Similarly, $CsPbBr_3$ PQDs in organic solvents detect Cu^{2+} with an LOD of 0.1 nM, leveraging OAm ligands for enhanced specificity.[62]

The characterization of $CsPbBr_3$ PQDs, as depicted in Fig. 9, provides a comprehensive analysis of their structural and optical properties.[62] Panels (a) and (f) present the absorption and PL spectra, respectively, showing a strong absorption peak around 510 nm and a corresponding PL emission peak, indicating the high optical quality of the PQDs dispersed in hexane under daylight and 365 nm UV lamp irradiation. The inset images in (a) visually confirm the uniform dispersion, while panel (b) offers a TEM image with a high-resolution TEM (HRTEM) inset, revealing a lattice spacing of 5.8 Å, consistent with the cubic phase of $CsPbBr_3$. These structural insights underscore the PQDs' crystallinity and potential for optoelectronic applications. Elemental composition and crystallographic structure are further elucidated in panels (c) and (d). Panel (c) displays the energy-dispersive X-ray spectroscopy (EDS) spectrum with an inset table detailing the atomic percentages (Cs: 20.2%, Pb: 34.83%, Br: 45.15%), confirming the stoichiometric ratio of the PQDs. Panel (d) shows the XRD pattern, matching the PDF # 54-0752 reference for the cubic phase, which aligns with the HRTEM findings and validates the phase purity of the synthesized $CsPbBr_3$ PQDs. These results highlight the material's compositional integrity and crystalline order, critical for its performance in heavy metal ion detection.

The comparison of $CsPbBr_3$ PQDs with and without Cu^{2+} ions is illustrated in panels (e) and (f). Panel (e) exhibits absorption spectra of $CsPbBr_3$ PQDs at different Cu^{2+} concentrations (0, 50, 100 nM), showing a gradual decrease in absorption intensity with increasing Cu^{2+}, indicative of ion-induced quenching. Panel (f) compares the PL spectra of pristine $CsPbBr_3$ PQDs and those with Cu-oleate, revealing a significant PL intensity drop upon Cu^{2+} addition, with an inset showing elemental ratios post-incubation. This quenching behavior is key to achieving ultra-low LODs, such as 0.1 nM for Cu^{2+}, as noted in the context of environmental monitoring applications. Panels (g) and (h) provide additional spectroscopic and kinetic data. Panel (g) presents the EDS spectrum of $CsPbBr_3$ aggregates with an inset table (Br: 48.35%, Cs: 18.64%, Pb: 31.81%), confirming the elemental composition after Cu^{2+} interaction. Panel (h) displays time-resolved PL decay curves at different Cu^{2+} concentrations (0, 50, 100 nM), with average lifetimes decreasing from 80.84 ns to 60.92 ns, reflecting enhanced non-radiative recombination due to Cu^{2+}. These kinetic changes correlate with the rapid response times (<10 s) and high sensitivity observed in lead-based PQDs for detecting heavy metal ions like Cu^{2+}, reinforcing their efficacy in practical sensing applications.

These systems excel in applications requiring high sensitivity, such as industrial solvent analysis. However, lead-based PQDs face significant challenges due to the toxicity of Pb^{2+}, which limits their use in environmentally sensitive applications. Their stability in aqueous media is often poor, necessitating advanced stabilization techniques. For example, $CsPbBr_3$ PQDs encapsulated in PCN-333(Fe) MOFs achieve an LOD of 1.63 nM for Cu^{2+} with improved stability and a 6.5-fold PL enhancement, suitable for water quality monitoring.[78] Encapsulation in ZIF-8 MOFs further extends stability to 15 days in aqueous solutions, with an LOD of 2.64 nM for Cu^{2+}.[79] Phase transfer methods using OAm also enable aqueous detection of Cu^{2+}, though complex synthesis and lead toxicity remain barriers to scalability.[61]

Lead-free PQDs, such as $Cs_3Bi_2X_9$ and $MASnBr_3$, offer environmentally friendly alternatives with enhanced stability in aqueous environments, critical for applications like wastewater and seawater analysis. Eu^{3+}-doped $Cs_3Bi_2Br_9$ PQDs detect Cu^{2+} with an LOD of 98.3 nM in seawater, benefiting from high photostability and moisture resistance.[60] $Cs_3Bi_2Cl_9$ PQDs, passivated with hydroxypropyl chitosan, achieve an LOD of 0.27 μM for Cr^{6+} in wastewater, supported by ligand-enhanced sensitivity.[71] These lead-free systems are ideal for eco-friendly industrial applications, particularly in marine and environmental monitoring. Despite their environmental advantages, lead-free PQDs typically exhibit lower PLQY (20–50%) and broader emission spectra, leading to higher LODs compared to lead-based systems. For example, $MASnBr_3$ PQDs with PEI ligands detect Fe^{3+} and Cr^{6+} in the nanomolar range but face stability challenges in harsh conditions.[68] $CsSnX_3$ PQDs achieve

 © 2025 The Author(s). Published by the Royal Society of Chemistry

Open Access Article. Published on 23 October 2025. Downloaded on 10/25/2025 7:28:42 PM.
This article is licensed under a Creative Commons Attribution 3.0 Unported Licence.

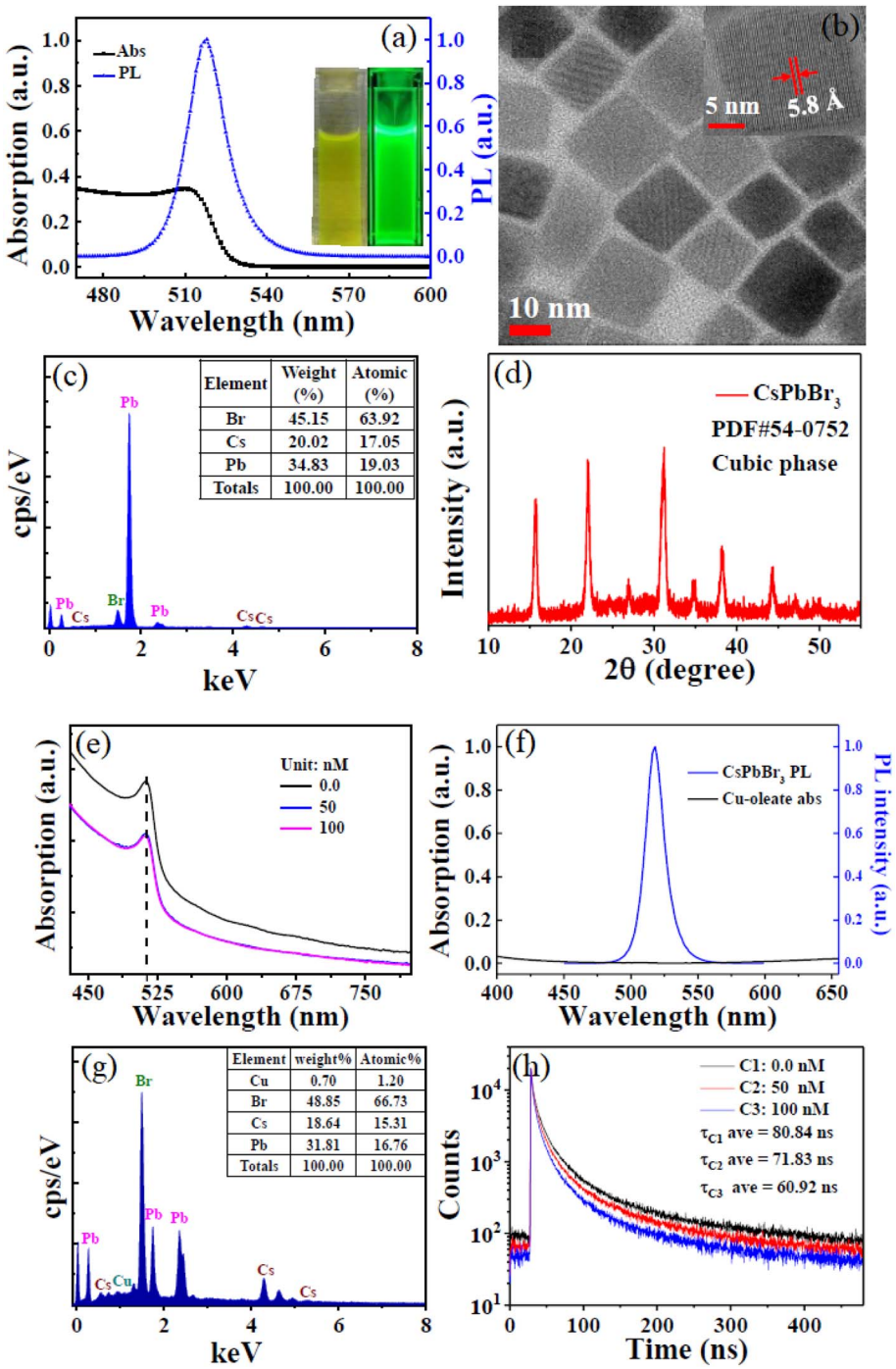

Fig. 9 Characterizations of $CsPbBr_3$ PQDs: (a) absorption and PL spectra, inset: images under daylight and 365 nm; (b) TEM and HRTEM inset; (c) EDS spectrum, inset: elemental ratios; (d) XRD pattern; (e) absorption spectra with Cu^{2+}; (f) PL spectrum with Cu-oleate; (g) EDS of aggregates, inset: ratios; (h) time-resolved PL decay, inset: lifetimes. Adapted with permission from ref. 62. Copyright 2018, Royal Society of Chemistry.

a low LOD of 3.5 nM for Pb^{2+} in organic solvents, yet Sn^{2+} oxidation limits their long-term stability.[75] These trade-offs make lead-free PQDs less competitive for ultra-sensitive applications but valuable for sustainable contexts.

Single-ion detection systems, such as $CH_3NH_3PbBr_3$ for Hg^{2+} (ref. 59) and $CsSnX_3$ for Pb^{2+},[75] provide high selectivity for specific heavy metal ions, making them suitable for targeted applications like lubricant quality control. In contrast, multi-ion sensors, such as Eu^{3+}-doped $Cs_3Bi_2Cl_6/Cs_3Bi_2Cl_9$ for Cu^{2+} and Fe^{3+} (LODs of 6.23 μM and 3.6 μM)[80] or $MASnBr_3$ for Fe^{3+} and Cr^{6+},[68] offer broader applicability but often at the expense of higher LODs. Ratiometric designs, like Mn^{2+}-doped $CsPbCl_3$ for Cu^{2+} (LOD 22.12 nM),[69] improve specificity in complex matrices through dual-emission signals. Lead-based PQDs are preferred

Open Access Article. Published on 23 October 2025. Downloaded on 10/25/2025 7:28:42 PM.
This article is licensed under a Creative Commons Attribution 3.0 Unported Licence.

Table 4 Comparative analysis of lead-based and lead-free PQD sensors for heavy metal ion detection

PQD type	Composition	Target ion	LOD	Selectivity	Stability	Application environment	Industrial applications	Advantages	Disadvantages	Ref.
Lead-based	$CH_3NH_3PbBr_3$	Hg^{2+}	0.124 nM	High (ionic radius similarity with Pb^{2+})	Moderate (moisture-sensitive)	Organic solvents (toluene)	Environmental monitoring	High PLQY (50.28%), rapid response (<10 s)	Lead toxicity, limited aqueous stability	59
Lead-based	$CsPbX_3$	Cu^{2+}	2 nM to 2 μM	Moderate (sensitive to transition metals)	Moderate (ligand-dependent)	Organic solvents (hexane)	Lubricants	Tunable bandgap, high sensitivity	Lead toxicity, poor aqueous stability	76
Lead-based	$CsPbBr_3$	Cu^{2+}	0.1 nM	High (oleylamine enhances coordination)	Moderate (stable in hexane)	Organic solvents (hexane)	Industrial solvents	Ultra-low LOD, fast response (<10 s)	Limited to non-aqueous media	62
Lead-based	$CsPbBr_3$	Cu^{2+}	Not specified	High (oleylamine enables phase transfer)	Improved in aqueous media	Aqueous solutions	Water quality monitoring	Aqueous compatibility	Lead toxicity, complex synthesis	61
Lead-based	$CsPbBr_3$ with Au nanoclusters	Cu^{2+}	Not specified	High (ratiometric design)	High (SiO_2 encapsulation)	Aqueous solutions	Environmental samples	Visual color change, high stability	Complex nanocomposite fabrication	64
Lead-based	$CsPbX_3$ in Zn-MOF	Cu^{2+}	Not specified	High (MOF enhances selectivity)	High (MOF encapsulation)	Aqueous solutions	Industrial wastewater	Enhanced stability, high PLQY	Scalability challenges for MOFs	81
Lead-based	$CsPbBr_3$ in PCN-333(Fe) MOF	Cu^{2+}	1.63 nM	High (MOF-mediated coordination)	High (6.5-fold PL enhancement)	Aqueous solutions	Environmental monitoring	Ultra-low LOD, enhanced PL	Lead toxicity, MOF synthesis complexity	78
Lead-based	$CsPbBr_3$@BBA	Cu^{2+}	0.8 μM	Moderate (ligand-mediated)	High (water-dispersible)	Aqueous solutions	Food safety	Water compatibility, high stability	Moderate LOD, lead toxicity	77
Lead-based	$CsPbBr_3$ in ZIF-8 MOF	Cu^{2+}	2.64 nM	High (MOF enhances specificity)	High (15 day stability in water)	Aqueous solutions	Water quality monitoring	Ultra-low LOD, long-term stability	Lead toxicity, complex MOF integration	79
Lead-based	$CsPbBr_3$–$CsPb_2Br_5$ with APTES	Fe^{3+}	10 μM	High (APTES reduces non-specific interactions)	High (APTES passivation)	Aqueous solutions	Industrial effluents	Fast response (8 s), high stability	Moderate LOD, lead toxicity	67
Lead-based	$CsPbBr_3$–$CsPb_2Br_5$ with ammonia hydroxide	Cd^{2+}	1 μM	Moderate (ammonia hydroxide enhances accessibility)	Moderate (aqueous compatibility)	Aqueous solutions	Industrial effluents	Improved aqueous detection	Moderate LOD, lead toxicity	72
Lead-free	$Cs_3Bi_2Br_9$:Eu^{3+}	Cu^{2+}	98.3 nM	High (Eu^{3+} doping enhances specificity)	High (stable in seawater)	Aqueous solutions (seawater)	Marine monitoring	Lead-free, high photostability	Lower PLQY (42.4%) than lead-based	60
Lead-free	$MASnBr_3$ with PEI	Fe^{3+}, Cr^{6+}	Nanomolar range	High (PEI chelation enhances selectivity)	Moderate (ligand-dependent)	Aqueous and organic solutions	Environmental monitoring	Lead-free, multi-ion detection	Limited stability in harsh conditions	68
Lead-free	$Cs_3Bi_2Cl_9$ with hydroxypropyl chitosan	Cr^{6+}	0.27 μM	High (chitosan enhances ion accessibility)	High (aqueous compatibility)	Aqueous solutions (wastewater)	Wastewater treatment	Lead-free, high sensitivity	Moderate LOD compared to lead-based	71
Lead-free	$Cs_3Bi_2Cl_6$/ $Cs_3Bi_2Cl_9$:Eu^{3+}	Cu^{2+}, Fe^{3+}	6.23 μM (Cu^{2+}), 3.6 μM (Fe^{3+})	Moderate (Eu^{3+} doping aids selectivity)	High (stable crystal structures)	Aqueous solutions	Environmental monitoring	Lead-free, multi-ion detection	Higher LOD than lead-based	80

© 2025 The Author(s). Published by the Royal Society of Chemistry

Open Access Article. Published on 23 October 2025. Downloaded on 10/25/2025 7:28:42 PM. This article is licensed under a Creative Commons Attribution 3.0 Unported Licence.

for applications demanding ultra-high sensitivity and rapid response, such as industrial solvent monitoring, but require advanced stabilization to overcome toxicity and aqueous instability. Lead-free PQDs excel in eco-friendly applications, particularly in aqueous environments like wastewater treatment, despite their lower sensitivity. Single-ion sensors offer high specificity, while multi-ion and ratiometric sensors provide versatility for complex systems. Future advancements should focus on enhancing the PLQY of lead-free PQDs, improving stability through novel ligands, and integrating computational tools to optimize sensor design for industrial scalability (Table 4).

4.4. Strategies for enhancing sensor performance

Several strategies have been developed to optimize the performance of PQD-based sensors, addressing limitations in stability, sensitivity, and selectivity for heavy metal detection.

4.4.1. Surface passivation and ligand engineering. Surface passivation with tailored ligands enhances stability and selectivity. Hydroxypropyl chitosan-passivated $Cs_3Bi_2Cl_9$ PQDs improve selectivity for Cr^{6+} by facilitating ion coordination, achieving an LOD of 0.27 μM in aqueous media.[71] APTES-coated $CsPbBr_3$–$CsPb_2Br_5$ PQDs enhance Fe^{3+} detection by reducing non-specific interactions, with an LOD of 10^{-5} M and a response time of 8 s.[67] Poly(ethylenimine) ligands in $MASnBr_3$ PQDs introduce chelating groups, improving Fe^{3+} selectivity through stable complex formation, critical for industrial fluid analysis.[68] These ligand designs optimize ion accessibility while maintaining PQD stability.

4.4.2. Encapsulation in stable matrices. Encapsulation in robust matrices, such as metal–organic frameworks (MOFs) or silica, protects PQDs from environmental degradation while maintaining analyte accessibility. $CsPbBr_3$ PQDs encapsulated in ZIF-8 MOFs achieve an LOD of 2.64 nM for Cu^{2+} and retain stability in water for 15 days, suitable for industrial wastewater monitoring.[79] PCN-333(Fe) MOF encapsulation enhances $CsPbBr_3$ stability, achieving an LOD of 1.63 nM for Cu^{2+} with a 6.5-fold PL enhancement.[78] Silica-encapsulated $CsPbBr_3$@-SiO_2 systems support ratiometric Cu^{2+} detection with high stability in aqueous environments, ideal for industrial applications.[64] These matrices balance protection and sensitivity, enabling robust sensor performance.[81]

4.4.3. Doping with metal ions. Doping with metal ions like Mn^{2+} or Eu^{3+} enhances PL stability and enables advanced sensing modalities. Mn^{2+}-doped $CsPbCl_3$ PQDs exhibit dual emission for ratiometric Cu^{2+} detection, achieving an LOD of 22.12 nM with a PLQY of 52.48%.[19] Eu^{3+}-doped $Cs_3Bi_2Br_9$ PQDs detect Cu^{2+} and Fe^{3+} with LODs of 6.23 μM and 3.6 μM, respectively, benefiting from improved photostability and polychromatic emission.[80] Doping introduces additional emission bands, enhancing detection accuracy in industrial settings.[66]

4.4.4. Ratiometric and visual sensing approaches. Ratiometric sensing improves accuracy by using dual-emission signals to mitigate environmental noise. $CsPbBr_3$ PQDs combined with Au nanoclusters enable ratiometric Cu^{2+} detection, with visual color changes enhancing usability in industrial quality control.[64] $Cs_3Bi_2Cl_9$ PQDs facilitate visual detection of Cr^{6+} at 0.27 μM through distinct PL changes, suitable for on-site industrial monitoring.[71]

4.5. Industrial applications of PQD-based nanosensors for heavy metal detection

PQD-based nanosensors have demonstrated significant potential in industrial settings for detecting heavy metal ions in various matrices, ensuring quality control and preventing contamination. These applications are particularly relevant in industries such as chemical processing, manufacturing, and waste management, where heavy metal pollutants pose significant risks to product integrity and environmental safety. $CsSnX_3$ PQDs are highly effective for detecting Pb^{2+} in lubricants and organic solutions, achieving an LOD of 3.5 nM through optimized synthesis methods that enhance PL stability.[75] Their design leverages the high compatibility of lead-free PQDs with non-aqueous media, making them ideal for monitoring industrial fluids used in machinery and automotive applications. The rapid response time (<15 s) and high selectivity over competing ions like Zn^{2+} or Ca^{2+} ensure reliable detection of trace Pb^{2+}, which is critical for maintaining lubricant quality and preventing equipment corrosion.[75] The robustness of $CsSnX_3$ PQDs in organic solvents, combined with their eco-friendly composition, positions them as a sustainable solution for industrial monitoring.

$CsPbX_3$ PQDs are employed to detect Cu^{2+} in organic solvents used in chemical processing, achieving a detection range of 2×10^{-9} to 2×10^{-6} M. Their high PLQY (up to 90%) and sensitivity make them suitable for monitoring trace Cu^{2+} in solvents used for catalysis or material synthesis, where even low concentrations can affect product quality.[76] For instance, Cu^{2+} contamination in organic solvents can catalyze unwanted side reactions, and PQD-based nanosensors provide a rapid and precise method to ensure solvent purity. The use of OAm ligands in these systems enhances selectivity by facilitating Cu^{2+} coordination, minimizing interference from other metal ions.[62] In industrial wastewater treatment, $Cs_3Bi_2Br_9$ PQDs are utilized to detect Cu^{2+} with an LOD of 98.3 nM, leveraging their high photostability and resistance to aqueous degradation.[60] These lead-free PQDs are particularly valuable in monitoring effluent streams from metal plating or electronics manufacturing, where Cu^{2+} contamination is a common concern. Their ability to function in aqueous environments without significant PL degradation makes them suitable for continuous monitoring systems, ensuring compliance with environmental regulations.[60] Additionally, hydroxypropyl chitosan-passivated $Cs_3Bi_2Cl_9$ PQDs detect Cr^{6+} in wastewater with an LOD of 0.27 μM, offering a visual detection method that is practical for on-site industrial applications.[71] The distinct PL changes induced by Cr^{6+} enable rapid identification of contamination, facilitating timely remediation.

$CsPbBr_3$–$CsPb_2Br_5$ PQDs, modified with ammonia hydroxide, are applied to detect Cd^{2+} in industrial effluents, achieving an LOD of 10^{-6} M. These sensors are designed for

Open Access Article. Published on 23 October 2025. Downloaded on 10/25/2025 7:28:42 PM. This article is licensed under a Creative Commons Attribution 3.0 Unported Licence.

wastewater from industries like battery manufacturing, where Cd^{2+} is a prevalent pollutant. The ammonia hydroxide modification enhances surface accessibility, improving sensitivity in aqueous media, which is critical for real-time monitoring of industrial discharge.[72] Similarly, APTES-coated $CsPbBr_3$–$CsPb_2Br_5$ PQDs detect Fe^{3+} with an LOD of 10^{-5} M, suitable for monitoring iron contamination in industrial fluids used in steel production or chemical synthesis.[67] The high stability of APTES coatings ensures reliable performance under harsh industrial conditions. Ratiometric sensing systems, such as $CsPbBr_3$ PQDs paired with Au nanoclusters, are employed for Cu^{2+} detection in industrial solvents, providing visual color changes that enhance usability for on-site quality control.[64] These systems are particularly valuable in industries requiring rapid, non-invasive detection methods, such as petrochemical processing, where Cu^{2+} contamination can degrade product performance. The dual-emission signals improve accuracy by mitigating environmental noise, ensuring precise quantification.[64]

5. Comparative analysis with other sensing materials for heavy metal ion detection

This section evaluates PQDs against alternative sensing materials, including carbon quantum dots (CQDs), graphene quantum dots (GQDs), traditional semiconductor quantum dots (*e.g.*, CdS, CdTe, ZnS-based), and metal–organic frameworks (MOFs), for detecting heavy metal ions. The comparison emphasizes performance metrics such as limit of detection (LOD), selectivity, PLQY, synthesis complexity, and applicability in environmental and industrial contexts. By benchmarking PQDs against these materials, their unique strengths, limitations, and synergistic potential are highlighted, ensuring a distinct perspective from prior mechanistic, design, and application discussions.

5.1. Comparative analysis of PQDs and nanomaterials for heavy metal sensing

Detecting heavy metal ions in environmental, industrial, and biological matrices requires materials with high sensitivity, selectivity, and practical applicability. PQDs, CQDs, GQDs, semiconductor quantum dots, and MOFs each offer distinct properties for this purpose. CQDs, derived from carbon-based precursors, feature surface functional groups (*e.g.*, NH_2, COOH) that enhance metal ion interactions, making them eco-friendly and suitable for aqueous environments.[82,83] GQDs, a subset of CQDs, leverage surface plasmon resonance (SPR) for detection, offering high stability in water.[84] Semiconductor QDs like CdS and CdTe provide tunable optical properties but are limited by toxicity.[85,86] MOFs, often paired with luminescent nanomaterials, enhance stability and selectivity through their porous structures.[78,87] Table 5 provides a comprehensive comparison of these materials' performance metrics, including LOD and PLQY, across various detection environments.

CQDs, synthesized *via* hydrothermal or microwave methods, typically exhibit PLQY of 20–50% and LODs of 5–35.8 nM for ions like Pb^{2+} and Hg^{2+} in water samples.[82,93] Their broad emission spectra limit sensitivity compared to PQDs. GQDs, with similar PLQY (20–30%), achieve LODs of 16.32 nM for Hg^{2+} using SPR, but their pyrolysis-based synthesis is less scalable.[84] Semiconductor quantum dots, such as CdTe, offer higher PLQY (50–60%) and LODs of 50–179.5 nM, but cadmium toxicity and complex synthesis hinder their use.[85,98] MOFs, while not inherently luminescent, enhance the performance of embedded fluorophores, though their fabrication is intricate.[78,87] PQDs combine high PLQY, narrow emission, and moderate synthesis complexity, making them versatile for both organic and aqueous applications. The choice of material depends on the application context. CQDs and GQDs excel in eco-friendly aqueous detection, while semiconductor QDs suit high-sensitivity needs despite toxicity concerns. MOFs enhance stability but require complex integration. PQDs offer a balanced profile of sensitivity, tunability, and adaptability, positioning them as a leading platform for heavy metal detection across diverse matrices.

5.2. Advantages of PQDs for heavy metal ion detection

PQDs, particularly lead-based variants like $CsPbX_3$ and $CH_3NH_3PbX_3$, exhibit exceptional optical properties, including high PLQY and narrow emission spectra, enabling ultra-low LODs (*e.g.*, 0.124 nM for Hg^{2+} with $CH_3NH_3PbBr_3$).[59] This optical precision supports ratiometric sensing, as seen in Mn^{2+}-doped $CsPbCl_3$ (LOD 22.12 nM for Cu^{2+}), enhancing accuracy in complex matrices.[69] Their tunable bandgap, adjusted *via* size or halide composition, allows tailored detection, such as $CsPbBr_3$ achieving an LOD of 0.1 nM for Cu^{2+} in hexane through OAm coordination.[62] Lead-free PQDs, like $Cs_3Bi_2Br_9$:Eu^{3+}, offer comparable performance (LOD 98.3 nM for Cu^{2+}) with reduced toxicity, ideal for aqueous environments like seawater.[89] Their rapid response times (<10 s) stem from efficient quenching mechanisms, such as cation exchange for Hg^{2+} detection with $CH_3NH_3PbBr_3$, outperforming CQDs' slower responses.[59,82] Integration into MOFs, as with $CsPbBr_3$@PCN-333(Fe) (LOD 1.63 nM for Cu^{2+}), enhances aqueous stability, making PQDs suitable for industrial wastewater monitoring.[78] Table 5 highlights these advantages, showing PQDs' superior LODs and versatility compared to other materials. PQDs' compatibility with organic solvents (*e.g.*, hexane, lubricants) and aqueous media *via* phase-transfer techniques (*e.g.*, oleylamine-modified $CsPbBr_3$, LOD 0.5 nM for Cu^{2+}) broadens their industrial applicability.[61] In contrast, GQDs are limited to aqueous systems, and CdS QDs struggle with selectivity in complex matrices.[84,98] The combination of high PLQY, tunability, and rapid response positions PQDs as a leading choice for high-performance heavy metal detection.

5.3. Limitations of alternative sensing materials

CQDs, despite their eco-friendliness, are constrained by lower PLQY (20–50%) and broader emission spectra, reducing sensitivity. For example, CQDs from blue crab shells achieve an LOD of 5 nM for Pb^{2+}, but their PLQY (50%) is lower than $CsPbBr_3$'s (81%).[62,83] Their need for complex surface functionalization to

 © 2025 The Author(s). Published by the Royal Society of Chemistry

Open Access Article. Published on 23 October 2025. Downloaded on 10/25/2025 7:28:42 PM.
This article is licensed under a Creative Commons Attribution 3.0 Unported Licence.

Table 5 Comparative performance of PQDs and other sensing materials for heavy metal ion detection

Material	Target ion	LOD	Selectivity	PLQY (%)	Synthesis complexity	Application environment	Ref.
$CH_3NH_3PbBr_3$ PQD	Hg^{2+}	0.124 nM	High (cation exchange)	50.28	Moderate (LARP)	Organic solvents (toluene)	59
$CH_3NH_3PbBr_3$@MOF-5 PQD	Cu^{2+}	0.5 nM	High (MOF-mediated coordination)	80	High (MOF encapsulation)	Aqueous solutions	87
$CsPbBr_3$/PMMA FM	Cu^{2+}	10^{-15} M	High (FRET-based)	88	High (electrospinning)	Aqueous/organic (ethanol solution)	88
$CsPbX_3$ PQD	Cu^{2+}, Yb^{3+}	2 nM	Moderate (transition metal sensitivity)	79	Moderate (hot-injection)	Organic solvents (hexane)	76
$CsPbBr_3$ PQD	Cu^{2+}	0.1 nM	High (oleylamine coordination)	81	Moderate (hot-injection)	Organic solvents (hexane)	62
$CsPbBr_3$ PQD (OAm phase transfer)	Cu^{2+}	0.5 nM	High (phase transfer enhances access)	80	High (phase transfer)	Aqueous solutions	61
$Cs_3Bi_2Br_9$:Eu^{3+} PQD	Cu^{2+}	98.3 nM	High (doping specificity)	42.4	Moderate (hydrothermal)	Aqueous (seawater)	89
$MASnBr_3$ PQD (PEI-capped)	Fe^{3+}, Cr^{6+}	1 nM	High (PEI chelation)	14.6	Moderate (LARP)	Aqueous/organic solutions	68
$CsPbCl_3$:Mn^{2+} PQD	Cu^{2+}	22.12 nM	High (ratiometric dual emission)	52.48	Moderate (hot-injection)	Aqueous solutions	69
$Cs_3Bi_2Cl_9$ PQD (chitosan-passivated)	Cr^{6+}	0.27 μM	High (ligand-enhanced coordination)	35	Moderate (hydrothermal)	Aqueous (wastewater)	71
$Cs_3Bi_2Cl_6$/ $Cs_3Bi_2Cl_9$:Eu^{3+} PQD	Cu^{2+}, Fe^{3+}	6.23 μM (Cu^{2+}), 3.6 μM (Fe^{3+})	Moderate (doping aids selectivity)	35	Moderate (hydrothermal)	Aqueous solutions	80
$CsSnX_3$ PQD	Pb^{2+}	3.5 nM	High (ligand-mediated specificity)	25	Moderate (hot-injection)	Organic solvents (lubricants)	75
$CsPbBr_3$@PCN-333(Fe) MOF PQD	Cu^{2+}	1.63 nM	High (MOF-mediated coordination)	85	High (MOF encapsulation)	Aqueous solutions	78
$CsPbBr_3$@ZIF-8 MOF PQD	Cu^{2+}	2.64 nM	High (MOF enhances specificity)	84	High (MOF encapsulation)	Aqueous solutions	79
$CsPbBr_3$–$CsPb_2Br_5$ PQD (APTES)	Fe^{3+}	10 μM	High (APTES reduces non-specificity)	85	Moderate (hot-injection)	Aqueous (industrial effluents)	67
$CsPbBr_3$–$CsPb_2Br_5$ PQD (NH_4OH)	Cd^{2+}	1 μM	Moderate (NH_4OH enhances access)	83	Moderate (hot-injection)	Aqueous (industrial effluents)	72
Carbon quantum dots (CQD thin film)	Pb^{2+}, Ni^{2+}, Mn^{2+}, Co^{2+}, Cr^{3+}	6 nM	Moderate (fluorescence quenching)	20	High (thin film deposition)	Aqueous (real water samples)	82
C_3B_2 quantum dots	Cd^{2+}, Hg^{2+}, Ni^{2+}, As^{3+}, Pb^{2+}	10 nM	High (>80% sensitivity, adsorption)	30	High (DFT-based design)	Aqueous (wastewater)	90
S@PSCA CQDs	Pb^{2+}, Ag^{+}	3.83 nM (Pb^{2+}), 9 μM (Ag^{+})	Moderate (colorimetric changes)	20	Moderate (hydrothermal)	Aqueous solutions	91
SO4@PSCA CQDs	Ag^{+}	8.2 nM	Moderate (colorimetric changes)	20	Moderate (hydrothermal)	Aqueous solutions	91
SnO_2 quantum dots	Ni^{2+}	10 nM	Moderate (Sn vacancy interactions)	25	Moderate (hydrolysis)	Aqueous (deionized, reclaimed, sea)	92
Nitrogen-doped CQDs (N-CQDs)	Fe^{3+}, Hg^{2+}	35.8 nM (Fe^{3+}), 6.8 nM (Hg^{2+})	High (fluorescence quenching)	20	High (oxidation)	Aqueous (pond, sea, well)	93
CQDs (blue crab shells)	Pb^{2+}, Hg^{2+}	5 nM	High (NH_2, COOH, OH groups)	50	Moderate (microwave)	Aqueous (aquaculture)	83

Open Access Article. Published on 23 October 2025. Downloaded on 10/25/2025 7:28:42 PM.
This article is licensed under a Creative Commons Attribution 3.0 Unported Licence.

Table 5 (*Contd.*)

Material	Target ion	LOD	Selectivity	PLQY (%)	Synthesis complexity	Application environment	Ref.
Graphene QDs (S,N-GQDs)	Hg^{2+}	16.32 nM	High (SPR-based)	30	Moderate (pyrolysis)	Aqueous (tap, river)	84
CdS QDs (DMSO-capped)	Cu^{2+}, Hg^{2+}, Pb^{2+}	179.5 nM (Cu^{2+}), 58 μM (Hg^{2+}), 60 μM (Pb^{2+})	High (colorimetric)	30	Moderate (chemical synthesis)	Aqueous (polluted samples)	85
CdTe QDs (TGA, GSH, L-cyst.)	Cr^{3+}, Pb^{2+}	100 nM	High (turn-on for Cr^{3+}, Pb^{2+})	58	Moderate (aqueous phase)	Aqueous/organic solutions	94
CdTe QDs (TGA-capped)	Cu^{2+}	50 nM	High (1 : 1 complexation)	60	Moderate (one-step aqueous)	Aqueous solutions	95
CdTe/CdS/ZnS QDs	Hg^{2+}	16.32 nM	High (fluorescence quenching)	59	High (multi-step aqueous)	Aqueous (tap, river, agricultural)	96
CdSe/ZnS QDs (TGA-capped)	Cr^{3+}, Cu^{2+}	100 nM	High (turn-off fluorescence)	60	Moderate (aqueous phase)	Aqueous solutions	97
CdS QDs (GSH-capped)	Cu^{2+}, Hg^{2+}, Mg^{2+}	100 nM	Moderate (fluorescence quenching)	59	Moderate (one-pot)	Foods (aqueous media)	98
CuInS2/ZnS QDs (GSH-capped)	Cu^{2+}	63 nM	High (aggregation-based quenching)	55	Moderate (aqueous)	Aqueous solutions	99
Co/Ag@ZnS QDs	Hg^{2+}	130 nM	High (fluorescence quenching)	27.6	Moderate (co-precipitation)	Aqueous (real water samples)	100
g-C_3N_4/CeO_2 heterostructure	Cu^{2+}, Hg^{2+}, Ag^{+}	26.2 μM, 17.5 μM, 14.9 μM	Moderate (binding affinity)	10	High (co-precipitation)	Aqueous solutions	101
Starch-capped CdS QD	Hg^{2+}, Cu^{2+}	100 nM	High (cation exchange reaction)	30	Moderate (aqueous)	Aqueous solutions	86

© 2025 The Author(s). Published by the Royal Society of Chemistry

Open Access Article. Published on 23 October 2025. Downloaded on 10/25/2025 7:28:42 PM.
This article is licensed under a Creative Commons Attribution 3.0 Unported Licence.

enhance selectivity increases synthesis complexity.[91,93] GQDs, with PLQY of 20–30%, achieve an LOD of 16.32 nM for Hg^{2+}, significantly higher than PQDs' 0.124 nM, and their pyrolysis synthesis is less scalable.[59,84] Semiconductor QDs like CdS and CdTe offer PLQY of 50–60% and LODs of 50–179.5 nM, but cadmium toxicity limits their environmental applications.[94–98] Their multi-step synthesis is more complex than PQD hot-injection or LARP methods, and selectivity often requires multiple capping agents.[94,97] MOFs, while enhancing stability when paired with PQDs, lack intrinsic luminescence and require intricate fabrication, limiting standalone use.[78,79] Table 5 underscores these limitations, showing higher LODs and synthesis challenges for alternative materials compared to PQDs' superior performance.

5.4. Synergistic approaches combining PQDs with other nanomaterials

Combining PQDs with MOFs, CQDs, or metal nanoclusters creates synergistic systems that enhance detection performance. Encapsulation in MOFs, such as $CsPbBr_3$@PCN-333(Fe) (LOD 1.63 nM for Cu^{2+}) or $CsPbBr_3$@ZIF-8 (LOD 2.64 nM), improves aqueous stability and analyte accessibility, ideal for wastewater monitoring.[78,79] These composites leverage MOF porosity and PQD optical properties, overcoming the aqueous instability of lead-based PQDs. Hybrid systems with CQDs or Au nanoclusters enable ratiometric sensing, as seen with $CsPbBr_3$ and Au nanoclusters for visual Cu^{2+} detection *via* FRET, enhancing accuracy in industrial solvents.[64] $CsPbBr_3$/PMMA fiber membranes achieve an LOD of 10^{-15} M for Cu^{2+}, combining PQD fluorescence with polymer matrix stability.[88] Doping with Eu^{3+} or Mn^{2+}, as in $Cs_3Bi_2Br_9$:Eu^{3+} (LOD 98.3 nM for Cu^{2+}), enhances PLQY and selectivity in aqueous settings.[69,89] These synergistic approaches address PQD limitations, offering performance superior to standalone CQDs or semiconductor quantum dots.

The provided figure illustrates key optical and energetic properties of Eu^{3+}-doped $Cs_3Bi_2Br_9$ PQDs combined with PeQD. Panel (a) presents the excitation spectra monitored at 446 nm and 620 nm, revealing distinct peaks at 365 nm and broader emissions influenced by Eu^{3+} doping, with emission wavelengths at 446 nm and 620 nm corresponding to transitions from the conduction band to the valence band and specific Eu^{3+} energy levels ($^5D_0 \rightarrow {}^7F_j$). This highlights the enhanced PL properties due to Eu^{3+} incorporation, which boosts PLQY and selectivity, as noted for $Cs_3Bi_2Br_9$:Eu^{3+} with an LOD of 98.3 nM for Cu^{2+}. Panel (b) depicts the energy level diagram, showing the alignment of Eu^{3+} levels ($^5D_0$ to $^5D_4$ and $^7F_0$ to $^7F_6$) with the conduction and valence bands of $Cs_3Bi_2Br_9$, facilitating efficient ET and FRET mechanisms that underpin the improved detection performance in hybrid systems. Panels (c) and (d) further

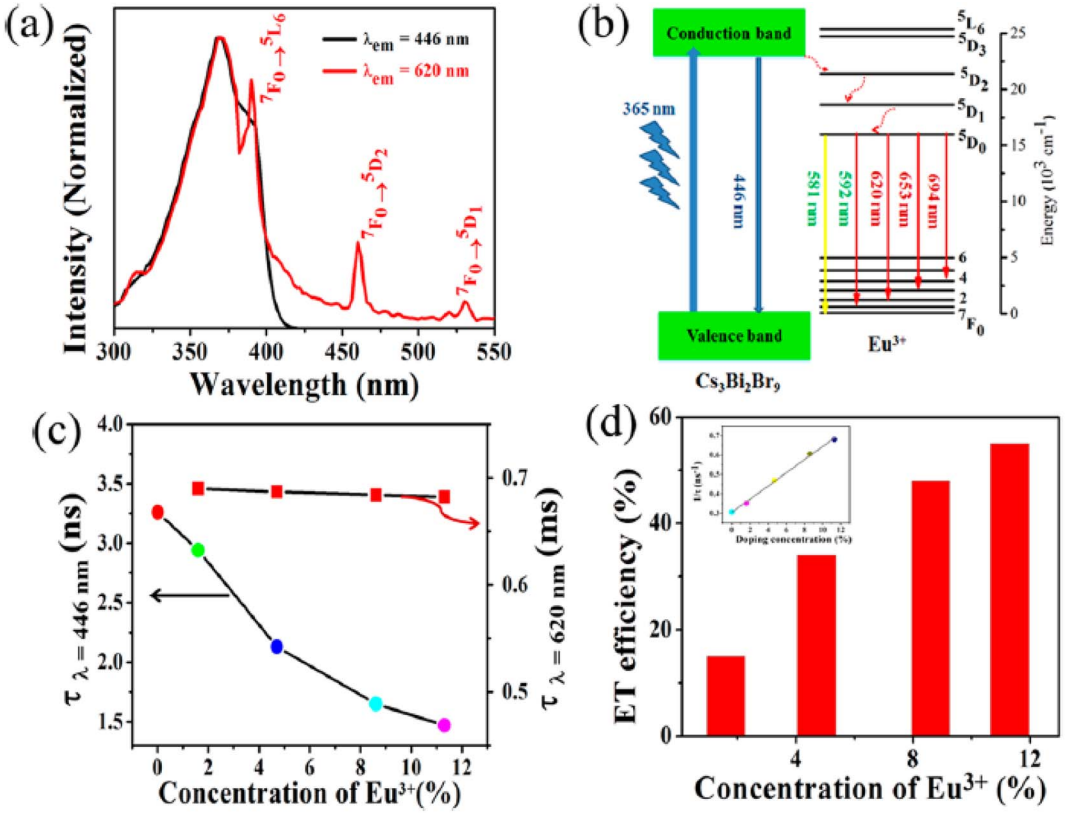

Fig. 10 (a) Excitation spectra of Eu^{3+} (8.6 mol%)-doped $Cs_3Bi_2Br_9$:PQDs at 446 and 620 nm. (b) Energy level diagram of Eu^{3+}-doped $Cs_3Bi_2Br_9$:PQDs. (c) Time-resolved PL decay at 446 nm and 620 nm ($^5D_0 \rightarrow {}^7F_j$) for undoped and Eu^{3+} (1.6–11.3 mol%)-doped samples. (d) Energy transfer efficiency from $Cs_3Bi_2Br_9$:PQDs to Eu^{3+} *vs.* concentration (inset: 446 nm decay constants). Reprinted with permission from ref. 89. Copyright 2019, American Chemical Society.

Open Access Article. Published on 23 October 2025. Downloaded on 10/25/2025 7:28:42 PM. This article is licensed under a Creative Commons Attribution 3.0 Unported Licence.

elucidate the concentration-dependent behavior of Eu^{3+} doping. Panel (c) shows the decay time (τ) at 446 nm decreasing from 3.5 ns to 1.5 ns with increasing Eu^{3+} concentration (0–12%), indicating enhanced non-radiative energy transfer to Eu^{3+} ions, as supported by the inset's reverse exciton emission decay constants. Panel (d) quantifies the ET efficiency (η_{ET}) and coefficient (α), peaking at 0.7 and 0.6, respectively, at 12% doping, alongside a bar graph of η_{ET}, which underscores the optimal doping level for maximizing PLQY and sensing accuracy in aqueous environments. These findings reinforce the synergistic potential of Eu^{3+}-doped PQDs with nanomaterials like MOFs or CQDs, enhancing stability and detection limits as demonstrated in systems like $CsPbBr_3$@PCN-333(Fe) and $CsPbBr_3$/PMMA fiber membranes (Fig. 10).

5.5. Benchmarking PQD performance against established sensors

PQDs consistently outperform alternative sensors in key metrics. For Hg^{2+}, $CH_3NH_3PbBr_3$ achieves an LOD of 0.124 nM, surpassing CdTe/CdS/ZnS (16.32 nM) and GQDs (16.32 nM) due to efficient cation exchange.[84,96] For Cu^{2+}, $CsPbBr_3$ reaches an LOD of 0.1 nM, compared to CdS (179.5 nM) and $CuInS_2$/ZnS (63 nM), leveraging rapid quenching mechanisms.[85,99] Lead-free $Cs_3Bi_2Cl_9$ detects Cr^{6+} at 0.27 μM, competitive with CdTe (100 nM), with added eco-friendliness.[71,94] PQDs' selectivity, enhanced by tailored ligands and doping, matches or exceeds that of CdTe and CdS, which require complex functionalization.[62,94] Their moderate synthesis complexity (hot-injection, LARP) contrasts with the multi-step processes of CdTe/CdS/ZnS or GQDs.[59,84] PQDs' versatility across organic and aqueous environments, particularly when integrated with MOFs, positions them as a robust platform for industrial and environmental monitoring, outperforming alternative materials in sensitivity and applicability.

6. Challenges, future directions, and pathways to industrial adoption

PQDs have emerged as a transformative platform for heavy metal ion detection, offering exceptional sensitivity, tunable optical properties, and versatility across diverse matrices. Despite their promise, several challenges hinder their practical implementation and scalability, particularly in environmental, industrial, and biomedical applications. Addressing these obstacles is essential to fully harness the potential of PQDs for detecting heavy metal ions such as Hg^{2+}, Cu^{2+}, Cd^{2+}, Fe^{3+}, Cr^{6+}, and Pb^{2+}. This section delineates the primary challenges associated with PQD-based nanosensors and proposes future directions to overcome these limitations, paving the way for advanced, reliable, and commercially viable detection systems.

6.1. Challenges in PQD-based heavy metal ion detection

6.1.1. Stability in aqueous and humid environments. The instability of PQDs, particularly lead-based variants like $CsPbX_3$ and $CH_3NH_3PbX_3$, in aqueous and humid environments remains a significant barrier. Exposure to moisture can degrade the perovskite lattice, leading to phase transitions or decomposition that diminish PLQY and sensing performance.[59,61] For instance, $CH_3NH_3PbBr_3$ PQDs exhibit reduced stability due to the volatility of organic cations, limiting their use in aqueous media such as wastewater or biological fluids.[59] While encapsulation in matrices like metal–organic frameworks (MOFs) or silica enhances stability, as seen with $CsPbBr_3$@ZIF-8 (stable for 15 days in water),[79] these approaches increase synthesis complexity and may compromise analyte accessibility, reducing sensitivity for ions like Cu^{2+} or Cr^{6+}.[78,79] Lead-free PQDs, such as $Cs_3Bi_2X_9$, offer improved moisture resistance but often at the cost of lower PLQY (20–50%), impacting detection limits.[60,71] Achieving robust stability without sacrificing optical performance remains a critical challenge for practical applications in industrial effluents and environmental monitoring.

6.1.2. Toxicity concerns of lead-based PQDs. The toxicity of lead-based PQDs, such as $CsPbX_3$ and $CH_3NH_3PbX_3$, poses significant environmental and health risks, particularly in applications involving water quality monitoring or biomedical diagnostics. The release of Pb^{2+} ions during degradation can contaminate the tested matrix, rendering these PQDs unsuitable for eco-sensitive applications.[59,62] Although lead-free alternatives like $Cs_3Bi_2X_9$ and $CsSnX_3$ mitigate toxicity concerns, their lower PLQY and stability issues, such as Sn^{2+} oxidation in $CsSnX_3$, limit their competitiveness.[68,75] For example, $Cs_3Bi_2Br_9$:Eu^{3+} achieves an LOD of 98.3 nM for Cu^{2+} in seawater, but its PLQY (42.4%) is significantly lower than that of $CsPbBr_3$ (81%).[60,62] Balancing toxicity reduction with high sensitivity and stability is a pressing challenge for widespread adoption.

6.1.3. Interference from coexisting ions and complex matrices. Selectivity in complex matrices, such as industrial wastewater or biological fluids, is hindered by interference from coexisting ions (*e.g.*, Na^+, K^+, Ca^{2+}) and organic species. While ligands like OAm or PE enhance selectivity for specific ions like Cu^{2+} or Fe^{3+}, non-specific interactions can lead to false positives or reduced sensitivity.[62,68] For instance, $CsPbBr_3$ PQDs show high selectivity for Cu^{2+} in hexane but face challenges in aqueous environments with multiple ions, where LODs increase from 0.1 nM to 0.8 μM.[77] Ratiometric designs, such as $CsPbBr_3$ with Au nanoclusters, mitigate some interference through dual-emission signals, but their complexity limits scalability.[64] Developing sensors that maintain high selectivity in real-world, multi-ion environments is a critical hurdle.

6.1.4. Scalability and reproducibility of sensor fabrication. The scalability of PQD synthesis and sensor fabrication remains challenging due to batch-to-batch variations in size, crystallinity, and ligand passivation. Methods like hot-injection yield high-quality PQDs with PLQY > 80%, but their high-temperature, inert-atmosphere requirements limit large-scale production.[62] Ligand-assisted reprecipitation (LARP) is more scalable but produces PQDs with broader size distributions and lower PLQY (50–70%), affecting reproducibility in sensing applications.[68] For example, variations in ligand density can alter ion accessibility, impacting the LOD for Cu^{2+} detection.[61] Additionally, integrating PQDs into stable matrices like MOFs or polymers increases fabrication complexity, posing challenges for cost-effective, industrial-scale production.[78,79] Ensuring

 © 2025 The Author(s). Published by the Royal Society of Chemistry

Open Access Article. Published on 23 October 2025. Downloaded on 10/25/2025 7:28:42 PM. This article is licensed under a Creative Commons Attribution 3.0 Unported Licence.

consistent sensor performance across large-scale manufacturing is essential for commercial applications.

6.1.5. Lack of standardization for commercial and regulatory applications. The absence of standardized protocols for PQD-based sensor design, calibration, and validation hinders their regulatory approval and commercial adoption. Variations in synthesis methods, ligand types, and detection conditions lead to inconsistent performance metrics, complicating comparisons across studies. For instance, LODs for Cu^{2+} detection range from 0.1 nM ($CsPbBr_3$ in hexane) to 6.23 μM ($Cs_3Bi_2Cl_6$:Eu^{3+} in aqueous media), reflecting diverse testing environments and sensor designs.[62,80] Regulatory frameworks for environmental and biomedical applications require standardized testing conditions and safety assessments, particularly for lead-based PQDs, which face scrutiny due to toxicity concerns.[59] Establishing universal standards for PQD-based nanosensors is critical to ensure reliability and compliance in practical settings.

6.2. Future directions for PQD-based sensors

To overcome the aforementioned challenges and advance PQD-based nanosensors for heavy metal ion detection, innovative strategies and interdisciplinary approaches are needed. The following directions outline opportunities to enhance stability, sensitivity, selectivity, and scalability, aligning with the demands of industrial, environmental, and biomedical applications.

6.2.1. Development of stable and eco-friendly lead-free PQDs. Advancing lead-free PQDs, such as $Cs_3Bi_2X_9$, $CsSnX_3$, or double perovskites (*e.g.*, $Cs_2AgInCl_6$), is crucial to address toxicity and stability concerns. Enhancing the PLQY of lead-free PQDs through doping with ions like Eu^{3+} or Mn^{2+} can improve sensitivity, as demonstrated by Eu^{3+}-doped $Cs_3Bi_2Br_9$ (LOD 98.3 nM for Cu^{2+}).[60] Novel synthesis methods, such as microwave-assisted or solvothermal approaches, can improve crystallinity and reduce defects, enhancing PLQY and stability in aqueous environments.[71] Exploring new compositions, such as germanium-based or antimony-based perovskites, could yield environmentally benign PQDs with optical properties comparable to lead-based systems, enabling sustainable applications in wastewater and seawater monitoring.

6.2.2. Advanced encapsulation and surface engineering. Innovative encapsulation strategies can enhance PQD stability without compromising analyte accessibility. Hybrid matrices combining MOFs with polymers or silica, such as $CsPbBr_3$@-PCN-333(Fe) (LOD 1.63 nM for Cu^{2+}), offer robust protection and high sensitivity.[78] Developing stimuli-responsive coatings that allow selective analyte penetration could further improve selectivity in complex matrices. Ligand engineering, such as using zwitterionic or multidentate ligands, can enhance water compatibility and ion-specific interactions, as seen with hydroxypropyl chitosan-passivated $Cs_3Bi_2Cl_9$ for Cr^{6+} detection (LOD 0.27 μM).[71] Machine learning-guided ligand design can optimize surface chemistry, predicting ligand–ion interactions to enhance selectivity and sensitivity for ions like Fe^{3+} or Cd^{2+}.

6.2.3. Integration with advanced detection platforms. Integrating PQD-based nanosensors with advanced platforms, such as microfluidics or smartphone-based systems, can enhance portability and real-time monitoring capabilities. Microfluidic devices can enable precise control over sample delivery, improving detection consistency in industrial effluents or biological fluids. For example, $CsPbBr_3$–$CsPb_2Br_5$ PQDs integrated into microfluidic chips could detect Cd^{2+} with high reproducibility.[72] Smartphone-based sensors, leveraging PQD fluorescence for visual or ratiometric detection, offer cost-effective solutions for on-site monitoring in industrial settings, as demonstrated by $CsPbBr_3$–Au nanocluster systems for Cu^{2+}.[64] These platforms can democratize access to high-sensitivity detection, particularly in resource-limited environments.

6.2.4. Machine learning and computational approaches. Machine learning (ML) and computational modeling, such as DFT and molecular dynamics (MD), can optimize PQD sensor design. ML algorithms can predict optimal PQD compositions and ligand configurations for specific ions, reducing experimental trial-and-error. For instance, DFT studies have elucidated Hg^{2+}-induced mid-gap states in $CH_3NH_3PbBr_3$, guiding sensor optimization.[59] ML-driven analysis of quenching mechanisms can enhance selectivity by identifying ion-specific interactions in complex matrices, improving performance for multi-ion detection.[80] Computational simulations can also model ion diffusion kinetics, informing ligand designs that balance stability and sensitivity, critical for detecting low-concentration ions like Pb^{2+} in lubricants.[75]

6.2.5. Standardization and scalable fabrication. Establishing standardized protocols for PQD synthesis, sensor calibration, and performance evaluation is essential for commercial and regulatory acceptance. Developing scalable synthesis methods, such as continuous-flow hot-injection or automated LARP systems, can improve reproducibility and reduce costs. For example, microwave-assisted synthesis offers rapid, uniform nucleation, suitable for large-scale production of $Cs_3Bi_2X_9$ PQDs.[71] Standardizing performance metrics, such as LOD and linear range, across diverse matrices (*e.g.*, organic solvents, wastewater) will facilitate comparisons and regulatory approval. Collaborative efforts between researchers, industry, and regulatory bodies can establish guidelines for PQD-based sensors, ensuring safety and reliability in applications like industrial wastewater treatment.

6.2.6. Multi-ion and multiplexed detection systems. Developing PQD-based nanosensors capable of detecting multiple heavy metal ions simultaneously will enhance their utility in complex industrial and environmental matrices. Multi-ion sensors, such as Eu^{3+}-doped $Cs_3Bi_2Cl_6$/$Cs_3Bi_2Cl_9$ for Cu^{2+} and Fe^{3+} detection (LODs 6.23 μM and 3.6 μM), demonstrate the potential for multiplexed systems.[80] Ratiometric designs with dual-emission PQDs, such as Mn^{2+}-doped $CsPbCl_3$, can improve accuracy by mitigating interference, ideal for industrial solvents or effluents.[69] Combining PQDs with other nanomaterials, like CQDs or metal nanoclusters, can enable multiplexed detection with visual readouts, enhancing usability in real-time quality

Open Access Article. Published on 23 October 2025. Downloaded on 10/25/2025 7:28:42 PM. This article is licensed under a Creative Commons Attribution 3.0 Unported Licence.

control.[64] Future research should focus on optimizing these systems for simultaneous detection of ions like Hg^{2+}, Cu^{2+}, and Cr^{6+}, addressing the needs of diverse applications.

6.2.7. Eco-friendly and biocompatible sensor designs. To address regulatory and environmental concerns, future PQD-based nanosensors should prioritize eco-friendly and biocompatible designs. Lead-free PQDs with enhanced PLQY and stability, such as doped $Cs_3Bi_2X_9$ or $Cs_2AgInCl_6$, can replace toxic lead-based systems in biomedical and environmental applications.[60] Biocompatible ligands, such as peptides or polysaccharides, can improve safety for biological fluid analysis, enabling detection of heavy metals in clinical settings. For instance, integrating $Cs_3Bi_2Cl_9$ with biocompatible coatings could enable Fe^{3+} detection in blood samples with minimal toxicity.[71] These advancements will broaden the applicability of PQD-based sensors, aligning with global sustainability goals.

6.3. Commercialization pathways and industrial integration

The transition of perovskite quantum dot (PQD)-based nanosensors from laboratory research to industrial applications requires strategic pathways to ensure scalability, cost-effectiveness, and seamless integration into existing industrial workflows. While PQD sensors demonstrate exceptional sensitivity and selectivity for heavy metal ion detection, their commercial adoption hinges on addressing economic, regulatory, and operational challenges, distinct from their technical performance in specific applications.

6.3.1. Cost-effective synthesis and manufacturing. Scaling up PQD synthesis for industrial use demands cost-effective methods that maintain high PLQY and reproducibility. Techniques like ligand-assisted reprecipitation (LARP) and continuous-flow hot-injection offer scalable alternatives to batch-based methods, reducing production costs while ensuring uniform PQD quality.[68] For instance, automating LARP processes could lower the cost of producing lead-free PQDs like $Cs_3Bi_2X_9$, making them economically viable for large-scale environmental monitoring.[60] Collaborative partnerships with chemical manufacturing industries can optimize precursor sourcing and waste management, further reducing costs. Additionally, developing modular synthesis platforms that integrate quality control metrics, such as real-time PLQY monitoring, can enhance batch consistency, addressing reproducibility concerns for commercial production.

6.3.2. Integration into industrial monitoring systems. Integrating PQD-based nanosensors into existing industrial systems, such as continuous monitoring platforms for wastewater treatment or quality control in chemical processing, requires compatibility with automated and IoT-enabled infrastructures. For example, embedding $CsPbBr_3$@ZIF-8 sensors into inline water quality analyzers can enable real-time detection of Cu^{2+} in industrial effluents, with data transmitted to centralized control systems.[79] Developing plug-and-play sensor modules that interface with standard industrial equipment, such as spectroscopy units or microfluidic systems, can streamline adoption. These modules should incorporate robust encapsulation (*e.g.*, MOFs or silica) to ensure stability under harsh industrial conditions, such as high temperatures or corrosive environments, without compromising analyte accessibility.[78]

6.3.3. Regulatory compliance and market readiness. Achieving regulatory approval for PQD-based nanosensors involves addressing safety and environmental concerns, particularly for lead-based PQDs. Lead-free PQDs, such as $Cs_3Bi_2Br_9$:Eu^{3+}, align better with environmental regulations due to their reduced toxicity, making them more viable for markets with stringent standards, such as the European Union's REACH framework.[60] Establishing standardized testing protocols for sensor performance, including LOD, selectivity, and stability under diverse conditions, is critical for regulatory acceptance. Collaborations with regulatory bodies can facilitate the development of certification pathways, ensuring PQD sensors meet industry standards for applications in wastewater treatment, chemical manufacturing, and environmental monitoring. Market readiness also requires demonstrating long-term reliability through field trials, such as deploying $CsSnX_3$ sensors in lubricant quality control systems to validate performance over extended periods.[75]

6.3.4. Economic viability and market differentiation. To compete with established sensing technologies, such as carbon QDs or semiconductor quantum dots, PQD-based nanosensors must offer clear economic advantages. Their high sensitivity (*e.g.*, LOD of 0.1 nM for Cu^{2+} with $CsPbBr_3$) and versatility across organic and aqueous media provide a competitive edge.[62] Positioning PQD sensors as cost-effective solutions for high-precision applications, such as detecting trace Pb^{2+} in lubricants, can attract industries seeking to minimize equipment downtime and contamination risks.[75] Developing portable, user-friendly devices, such as smartphone-integrated PQD sensors for on-site Cu^{2+} detection, can target niche markets like small-scale chemical processing or environmental consulting, enhancing market penetration.[64] Strategic partnerships with sensor manufacturers and distributors can accelerate market entry, leveraging existing supply chains to reduce time-to-market.

7. Conclusion

This comprehensive review underscores the transformative potential of PQDs as advanced platforms for heavy metal ion detection, marking the first systematic evaluation of their application in this domain. PQDs, with their high photoluminescence quantum yield, narrow emission spectra, and tunable optical properties, offer unparalleled sensitivity and selectivity for detecting ions such as Hg^{2+}, Cu^{2+}, Cd^{2+}, Fe^{3+}, Cr^{6+}, and Pb^{2+}. Their efficacy, driven by mechanisms like cation exchange and electron transfer, is enhanced by advanced synthesis methods and integration with stable matrices like metal–organic frameworks. Lead-based PQDs achieve sub-nanomolar detection limits, while lead-free variants address environmental concerns, broadening their applicability. The versatility of PQDs enables their use in industrial wastewater treatment and lubricant quality control, ensuring compliance with environmental regulations and product integrity. Despite

 © 2025 The Author(s). Published by the Royal Society of Chemistry

Open Access Article. Published on 23 October 2025. Downloaded on 10/25/2025 7:28:42 PM.
This article is licensed under a Creative Commons Attribution 3.0 Unported Licence.

these advancements, challenges such as aqueous instability, toxicity of lead-based PQDs, and scalability of synthesis methods remain. Future research should focus on developing stable, eco-friendly PQDs through novel encapsulation techniques and ligand designs, alongside computational modeling to optimize ion–PQD interactions. Comparative studies with other nanomaterials, such as carbon quantum dots, will further elucidate their unique advantages. By addressing these challenges, PQDs can transition from laboratory innovations to practical sensing solutions, offering rapid, cost-effective, and portable detection for environmental and industrial applications. This review lays a foundation for advancing PQD-based sensors, guiding researchers toward innovations that enhance sensitivity, selectivity, and scalability, ultimately contributing to sustainable monitoring of heavy metal ion contamination.

Author contributions

Ahmad Mohebi and Suleiman Ibrahim Mohammad conceptualized the study. Asokan Vasudevan, I. B. Sapaev, and Munthar Kadhim Abosaoda developed the methodology. Chou-Yi Hsu, Malatesh Akkur, and Alok Kumar Mishra conducted the investigation. Gaganjot Kaur and Rajesh Singh handled data curation. Suleiman Ibrahim Mohammad and Ahmad Mohebi drafted the original manuscript, while Ahmad Mohebi, Asokan Vasudevan, and Chou-Yi Hsu reviewed and edited it. I. B. Sapaev and Munthar Kadhim Abosaoda contributed to visualization. Ahmad Mohebi supervised and managed the project. Suleiman Ibrahim Mohammad secured funding. All authors have read and agreed to the published version of the manuscript.

Conflicts of interest

There are no conflicts to declare.

Data availability

No primary research results, software or code have been included and no new data were generated or analysed as part of this review.

Acknowledgements

The research is funded by Zarqa University.

References

1 Y. Han, S. Zhang, D. Kang, N. Hao, J. Peng, Y. Zhou, K. Liu and Y. Chen, A Decade Review of Human Health Risks from Heavy Metal Contamination in Industrial Sites, *Water, Air, Soil Pollut.*, 2025, **236**(2), 144.
2 S. Syarifuddin, S. Suryani and D. Tahir, Global advances and innovations in bacteria-based biosorption for heavy metal remediation: a bibliometric and analytical perspective, *Integrated Environ. Assess. Manag.*, 2025, **21**(3), 507–525.
3 M. Swathika, N. M. Andal, S. Dharani, J. Singh, S. S. Pandey, K. R. Singh and A. Natarajan, Targeted elimination of heavy metals from industrial wastewater: synergistic effect of nano metal oxides, *J. Taiwan Inst. Chem. Eng.*, 2025, **166**, 105485.
4 R. U. Khan, M. Hamayun, A. A. Altaf, S. Kausar, Z. Razzaq and T. Javaid, Assessment and removal of heavy metals and other ions from the industrial wastewater of Faisalabad, Pakistan, *Processes*, 2022, **10**(11), 2165.
5 H. Sable, V. Kumar, V. Singh, S. Rustagi, S. Chahal and V. Chaudhary, Strategically engineering advanced nanomaterials for heavy-metal remediation from wastewater, *Coord. Chem. Rev.*, 2024, **518**, 216079.
6 A. T. Ahmed, F. M. Altalbawy, H. R. Al-Hetty, N. Fayzullaev, K. V. Jamuna, J. Sharma, B. Abd, A. M. Ahmed and H. Noorizadeh, Cadmium selenide quantum dots in photo-and electrocatalysis: advances in hydrogen, oxygen, and CO2 reactions, *Mater. Sci. Semicond. Process.*, 2025, **199**, 109831.
7 S. Anwar, Q. A. Syed, A. Ullah, M. Arshad, S. N. Khan and M. I. Hussain, Detection of heavy metals using atomic absorption and emission spectroscopy in drinking water of Faisalabad, Pakistan: microbial safety and quality status assessment, *Toxin Rev.*, 2024, **43**(1), 1–7.
8 M. H. Abdellattif, H. Noorizadeh, S. Al-Hasnaawei, S. Ganesan, A. F. Al-Hussainy, A. Sandhu, A. Sinha and M. Kazemi, Tailoring Charge Storage Mechanisms through TiO_2 Quantum Dots: A Multifunctional Strategy for High-Performance Battery Electrodes, *Surf. Interfaces*, 2025, **9**, 107164.
9 J. Y. Cai, H. Shen, J. N. Xu, J. M. Xu, J. H. Wang and Y. L. Yu, Magnetic Field-Accelerated Nonthermal Plasma Digestion for Field Pretreatment and Determination of Heavy Metals in Biological Samples, *Anal. Chem.*, 2025, **97**(5), 2899–2905.
10 Y. Shi, S. Zhang, H. Zhou, Y. Dong, G. Liu, W. Ye, R. He and G. Zhao, Recent Developments in Heavy Metals Detection: Modified Electrodes, Pretreatment Methods, Prediction Models and Algorithms, *Metals*, 2025, **15**(1), 80.
11 Z. Lian and F. Y. Kong, Treatments of Heavy Metals in Bio Electrochemical Systems (BES) and Microbial Transfer Mechanisms: Analyses of Influencing Factors, Future Research Directions, Prospect and Outlook, *Water, Air, Soil Pollut.*, 2025, **236**(8), 1–39.
12 S. Y. Kew and S. Y. Lau, Review on electrochemical reactors for efficient heavy metals removal from wastewater, *J. Ind. Eng. Chem.*, 2025, **152**, 18–32.
13 T. Hu, Q. Lai, W. Fan, Y. Zhang and Z. Liu, Advances in portable heavy metal ion sensors, *Sensors*, 2023, **23**(8), 4125.
14 M. F. Rauf, Z. Lin, M. K. Rauf and J. M. Lin, Innovative Microfluidic Technologies for Rapid Heavy Metal Ion Detection, *Chemosensors*, 2025, **13**(4), 149.
15 H. Zhang, L. Li, C. Wang, Q. Liu, W. T. Chen, S. Gao and G. Hu, Recent advances in designable nanomaterial-based electrochemical sensors for environmental heavy-metal detection, *Nanoscale*, 2025, **17**, 2386–2407.
16 C. W. Hsieh, R. K. Singh, M. L. Meena, S. A. Lu, K. K. Gupta, B. C. Lin and C. H. Lu, Development of inorganic perovskite quantum dots-based optical sensor for toxic Cd2+ metal ion detection, *Optik*, 2025, **22**, 172462.

Open Access Article. Published on 23 October 2025. Downloaded on 10/25/2025 7:28:42 PM.
This article is licensed under a Creative Commons Attribution 3.0 Unported Licence.

17 M. Kedhim, V. Jain, S. Ballal, A. Kumar, A. Singh, V. Kavitha, R. Panigrahi and H. Noorizadeh, Ultrasensitive dopamine detection using CsPbBr 3-PQD-COF nanocomposites: a synergistic fluorescence and EIS approach, *RSC Adv.*, 2025, **15**(24), 18875–18892.
18 X. Zhang, L. Li, Y. Chen, C. Valenzuela, Y. Liu, Y. Yang, Y. Feng, L. Wang and W. Feng, Mechanically tunable circularly polarized luminescence of liquid crystal-templated chiral perovskite quantum dots, *Angew. Chem.*, 2024, **136**(22), e202404202.
19 B. Xu, S. Yuan, L. Wang, X. Li, Z. Hu and H. Zeng, Highly Efficient Blue Light-Emitting Diodes Enabled by Gradient Core/Shell-Structured Perovskite Quantum Dots, *ACS Nano*, 2025, **19**(3), 3694–3704.
20 J. W. Choi, H. C. Woo, X. Huang, W. G. Jung, B. J. Kim, S. W. Jeon, S. Y. Yim, J. S. Lee and C. L. Lee, Organic–inorganic hybrid perovskite quantum dots with high PLQY and enhanced carrier mobility through crystallinity control by solvent engineering and solid-state ligand exchange, *Nanoscale*, 2018, **10**(28), 13356–13367.
21 W. Chen, X. Xin, Z. Zang, X. Tang, C. Li, W. Hu, M. Zhou and J. Du, Tunable photoluminescence of CsPbBr3 perovskite quantum dots for light emitting diodes application, *J. Solid State Chem.*, 2017, **255**, 115–120.
22 Q. Shan, Y. Dong, H. Xiang, D. Yan, T. Hu, B. Yuan, H. Zhu, Y. Wang and H. Zeng, Perovskite quantum dots for the next-generation displays: progress and prospect, *Adv. Funct. Mater.*, 2024, **34**(36), 2401284.
23 M. Shellaiah, K. Awasthi, S. Chandran, B. Aazaad, K. W. Sun, N. Ohta, S. P. Wu and M. C. Lin, Methylammonium tin tribromide quantum dots for heavy metal ion detection and cellular imaging, *ACS Appl. Nano Mater.*, 2022, **5**(2), 2859–2874.
24 K. Tang, Y. Chen and Y. Zhao, Exploiting halide perovskites for heavy metal ion detection, *Chem. Commun.*, 2024, **60**(34), 4511–4520.
25 H. Ye, W. Gao and L. Xu, High-temperature energy storage capability of polyetherimide composite incorporated with perovskite quantum dots, *Colloids Surf., A*, 2024, **687**, 133479.
26 H. Huang, J. Zhou, Q. Cai, C. Zhou, N. Li, X. Dai, Z. Ye, H. He and C. Fan, Industrial-Scale Fabrication of Mixed-Halide Perovskite Quantum Dots with High Comprehensive Performances for Red-Emitting Modules, *Nano Lett.*, 2025, **25**(24), 9863–9871.
27 X. G. Wu, Y. Jing and H. Zhong, In Situ Fabricated Perovskite Quantum Dots: From Materials to Applications, *Adv. Mater.*, 2024, 2412276.
28 P. Sun, Z. Xing, Z. Li and W. Zhou, Recent advances in quantum dots photocatalysts, *Chem. Eng. J.*, 2023, **458**, 141399.
29 S. Aftab, Z. Ali, M. I. Hussain, M. A. Assiri, N. Rubab, F. Ozel and E. Akman, Perovskite Quantum Dots: Fabrication, Degradation, and Enhanced Performance Across Solar Cells, Optoelectronics, and Quantum Technologies, *Carbon Energy*, 2025, e70018.
30 J. Lin, S. Chen, W. Ye, Y. Zeng, H. Xiao, T. Pang, Y. Zheng, B. Zhuang, F. Huang and D. Chen, Ultra-stable yellow monolithic perovskite quantum dots film for backlit display, *Adv. Funct. Mater.*, 2024, **34**(27), 2314795.
31 X. Wang, Z. Bao, Y. C. Chang and R. S. Liu, Perovskite quantum dots for application in high color gamut backlighting display of light-emitting diodes, *ACS Energy Lett.*, 2020, **5**(11), 3374–3396.
32 J. Zhang, S. Zhang, Y. Zhang, O. A. Al-Hartomy, S. Wageh, A. G. Al-Sehemi, Y. Hao, L. Gao, H. Wang and H. Zhang, Colloidal quantum dots: synthesis, composition, structure, and emerging optoelectronic applications, *Laser Photon. Rev.*, 2023, **17**(3), 2200551.
33 J. Zou, M. Li, X. Zhang and W. Zheng, Perovskite quantum dots: synthesis, applications, prospects, and challenges, *J. Appl. Phys.*, 2022, **132**(22), 220901.
34 Z. Ning, X. Gong, R. Comin, G. Walters, F. Fan, O. Voznyy, E. Yassitepe, A. Buin, S. Hoogland and E. H. Sargent, Quantum-dot-in-perovskite solids, *Nature*, 2015, **523**(7560), 324–328.
35 A. Soosaimanickam, A. Saura, N. Farinós and R. Abargues, Influence of binary ligands in designing cesium lead halide (CsPbX3, X= Cl, Br, I) perovskite nanocrystals-oleic acid and oleylamine, *Nanoenergy Adv.*, 2023, **3**(4), 376–400.
36 N. S. Makarov, S. Guo, O. Isaienko, W. Liu, I. Robel and V. I. Klimov, Spectral and dynamical properties of single excitons, biexcitons, and trions in cesium–lead-halide perovskite quantum dots, *Nano Lett.*, 2016, **16**(4), 2349–2362.
37 Y. Zhou and Y. Wang, Perovskite Quantum Dots, *Springer Series in Materials Science*, 2020.
38 Y. Zhu, J. Zhu, H. Song, J. Huang, Z. Lu and G. Pan, Samarium doping improves luminescence efficiency of Cs3Bi2Br9 perovskite quantum dots enabling efficient white light-emitting diodes, *J. Rare Earths*, 2021, **39**(4), 374–379.
39 Y. Tang, S. Tang, M. Luo, Y. Guo, Y. Zheng, Y. Lou and Y. Zhao, All-inorganic lead-free metal halide perovskite quantum dots: progress and prospects, *Chem. Commun.*, 2021, **57**(61), 7465–7479.
40 D. E. Lee, S. Y. Kim and H. W. Jang, Lead-free all-inorganic halide perovskite quantum dots: review and outlook, *J. Korean Ceram. Soc.*, 2020, **57**(5), 455–479.
41 D. Wu, F. Zhou, K. Feng, J. Wang, Q. Lu, X. Wang, Z. Zhan, W. Chen, Z. Liu, Z. Zhang and Z. Hu, Rare earth Nd3+-doped organic-inorganic hybrid perovskite quantum dots for white LED, *J. Lumin.*, 2025, **277**, 120876.
42 J. W. Choi, H. C. Woo, X. Huang, W. G. Jung, B. J. Kim, S. W. Jeon, S. Y. Yim, J. S. Lee and C. L. Lee, Organic–inorganic hybrid perovskite quantum dots with high PLQY and enhanced carrier mobility through crystallinity control by solvent engineering and solid-state ligand exchange, *Nanoscale*, 2018, **10**(28), 13356–13367.
43 M. Leng, Y. Yang, K. Zeng, Z. Chen, Z. Tan, S. Li, J. Li, B. Xu, D. Li, M. P. Hautzinger and Y. Fu, All-inorganic bismuth-based perovskite quantum dots with bright blue

 © 2025 The Author(s). Published by the Royal Society of Chemistry

Open Access Article. Published on 23 October 2025. Downloaded on 10/25/2025 7:28:42 PM.
This article is licensed under a Creative Commons Attribution 3.0 Unported Licence.

photoluminescence and excellent stability, *Adv. Funct. Mater.*, 2018, **28**(1), 1704446.

44 E. Jokar, L. Cai, J. Han, E. J. Nacpil and I. Jeon, Emerging opportunities in lead-free and lead–tin perovskites for environmentally viable photodetector applications, *Chem. Mater.*, 2023, **35**(9), 3404–3426.

45 T. Wu, X. Liu, X. Luo, X. Lin, D. Cui, Y. Wang, H. Segawa, Y. Zhang and L. Han, Lead-free tin perovskite solar cells, *Joule*, 2021, **5**(4), 863–886.

46 Z. Long, S. Yang, J. Pi, D. Zhou, Q. Wang, Y. Yang, H. Wu and J. Qiu, All-inorganic halide perovskite (CsPbX3, X= Cl, Br, I) quantum dots synthesized via fast anion hot injection by using trimethylhalosilanes, *Ceram. Int.*, 2022, **48**(23), 35474–35479.

47 F. Meng, X. Liu, X. Cai, Z. Gong, B. Li, W. Xie, M. Li, D. Chen, H. L. Yip and S. J. Su, Incorporation of rubidium cations into blue perovskite quantum dot light-emitting diodes via FABr-modified multi-cation hot-injection method, *Nanoscale*, 2019, **11**(3), 1295–1303.

48 S. Aftab, A. Shah, C. Erkmen, S. Kurbanoglu and B. Uslu, Quantum dots: synthesis and characterizations, in *Electroanalytical Applications of Quantum Dot-Based Biosensors*, Elsevier, 2021, pp. 1–35.

49 J. Zou, M. Li, X. Zhang and W. Zheng, Perovskite quantum dots: synthesis, applications, prospects, and challenges, *J. Appl. Phys.*, 2022, **132**(22), 220901.

50 C. Bi, S. Wang, W. Wen, J. Yuan, G. Cao and J. Tian, Room-temperature construction of mixed-halide perovskite quantum dots with high photoluminescence quantum yield, *J. Phys. Chem. C*, 2018, **122**(9), 5151–5160.

51 S. Mandal, D. Roy, C. K. De, S. Ghosh, M. Mandal, A. Das and P. K. Mandal, Instantaneous, room-temperature, open-air atmosphere, solution-phase synthesis of perovskite quantum dots through halide exchange employing non-metal based inexpensive HCl/HI: ensemble and single particle spectroscopy, *Nanoscale Adv.*, 2019, **1**(9), 3506–3513.

52 Y. Li, H. Huang, Y. Xiong, S. V. Kershaw and A. L. Rogach, Revealing the formation mechanism of CsPbBr3 perovskite nanocrystals produced via a slowed-down microwave-assisted synthesis, *Angew. Chem., Int. Ed.*, 2018, **57**(20), 5833–5837.

53 C. H. Lu, Y. H. Liu, M. L. Meena and S. Som, Synthesis and spectroscopic characterization of CsPbBr3/Cs4PbBr6 perovskites synthesized via the microwave-assisted heating process for backlight display devices, *Org. Electron.*, 2021, **91**, 106079.

54 M. Guarino-Hotz, J. L. Barnett, L. B. Pham, A. A. Win, V. L. Cherrette and J. Z. Zhang, Tuning between methylammonium lead bromide perovskite magic-sized clusters and quantum dots through ligand assisted reprecipitation at elevated temperatures, *J. Phys. Chem. C*, 2022, **126**(32), 13854–13862.

55 S. L. Sanchez, Y. Tang, B. Hu, J. Yang and M. Ahmadi, Understanding the ligand-assisted reprecipitation of CsPbBr3 nanocrystals via high-throughput robotic synthesis approach, *Matter*, 2023, **6**(9), 2900–2918.

56 Q. Zhao, S. Wang, Y. H. Kim, S. Mondal, Q. Miao, S. Li, D. Liu, M. Wang, Y. Zhai, J. Gao and A. Hazarika, Advantageous properties of halide perovskite quantum dots towards energy-efficient sustainable applications, *Green Energy Environ.*, 2024, **9**(6), 949–965.

57 D. Chen and X. Chen, Luminescent perovskite quantum dots: synthesis, microstructures, optical properties and applications, *J. Mater. Chem. C*, 2019, **7**(6), 1413–1446.

58 Y. Bai, M. Hao, S. Ding, P. Chen and L. Wang, Surface chemistry engineering of perovskite quantum dots: strategies, applications, and perspectives, *Adv. Mater.*, 2022, **34**(4), 2105958.

59 L. Q. Lu, T. Tan, X. K. Tian, Y. Li and P. Deng, Visual and sensitive fluorescent sensing for ultratrace mercury ions by perovskite quantum dots, *Anal. Chim. Acta*, 2017, **986**, 109–114.

60 Y. Gao and B. Chen, Lead-free Cs3Bi2Br9 perovskite quantum dots for detection of heavy metal Cu2+ ions in seawater, *J. Mar. Sci. Eng.*, 2023, **11**(5), 1001.

61 Q. Li, W. Zhou, L. Yu, S. Lian and Q. Xie, Perovskite quantum dots as a fluorescent probe for metal ion detection in aqueous solution via phase transfer, *Mater. Lett.*, 2021, **282**, 128654.

62 Y. Liu, X. Tang, T. Zhu, M. Deng, I. P. Ikechukwu, W. Huang, G. Yin, Y. Bai, D. Qu, X. Huang and F. Qiu, All-inorganic CsPbBr 3 perovskite quantum dots as a photoluminescent probe for ultrasensitive Cu 2+ detection, *J. Mater. Chem. C*, 2018, **6**(17), 4793–4799.

63 J. Iskandar, C. Y. Liu, C. C. Lee, K. Y. Ke, M. R. Septian, R. Estrada, H. Humaidi, S. Biring, C. S. Chu, Z. L. Tseng and S. W. Liu, Stabilizing perovskite quantum dot oxygen sensors through ultra-long 2 mm horizontally aligned nanopores in anodic alumina oxide templates, *J. Mater. Chem. C*, 2025, **13**(2), 709–717.

64 W. Xue, J. Zhong, H. Wu, J. Zhang and Y. Chi, A visualized ratiometric fluorescence sensing system for copper ions based on gold nanoclusters/perovskite quantum dot@ SiO 2 nanocomposites, *Analyst*, 2021, **146**(24), 7545–7553.

65 K. Tang, Y. Chen and Y. Zhao, Exploiting halide perovskites for heavy metal ion detection, *Chem. Commun.*, 2024, **60**(34), 4511–4520.

66 M. Shellaiah, K. W. Sun, N. Thirumalaivasan, M. Bhushan and A. Murugan, Sensing utilities of cesium lead halide perovskites and composites: a comprehensive review, *Sensors*, 2024, **24**(8), 2504.

67 C. W. Hsieh, R. K. Singh, S. Som and C. H. Lu, Detection of Fe (III) using APTES-coated CsPbBr3–CsPb2Br5 perovskite quantum dots, *Chem. Eng. J. Adv.*, 2022, **12**, 100358.

68 M. Shellaiah, K. Awasthi, S. Chandran, B. Aazaad, K. W. Sun, N. Ohta, S. P. Wu and M. C. Lin, Methylammonium tin tribromide quantum dots for heavy metal ion detection and cellular imaging, *ACS Appl. Nano Mater.*, 2022, **5**(2), 2859–2874.

69 Y. Gao, S. Xu, Y. Li and B. Chen, Mn-doped CsPbCl3 perovskite quantum dots: a dual-function probe for copper detection and temperature sensing, *Spectrochim. Acta, Part A*, 2025, **326**, 125219.

Open Access Article. Published on 23 October 2025. Downloaded on 10/25/2025 7:28:42 PM.
This article is licensed under a Creative Commons Attribution 3.0 Unported Licence.

70 P. Pandey, A. Sengupta, S. Parmar, U. Bansode, S. Gosavi, A. Swarnkar, S. Muduli, A. D. Mohite and S. Ogale, CsPbBr3–Ti3C2T x MXene QD/QD heterojunction: photoluminescence quenching, charge transfer, and Cd ion sensing application, *ACS Appl. Nano Mater.*, 2020, **3**(4), 3305–3314.

71 D. Gao, A. Zhang, B. Lyu and J. Ma, Visual and rapid fluorescence sensing for hexavalent chromium by hydroxypropyl chitosan passivated bismuth-based perovskite quantum dots, *Microchim. Acta*, 2024, **191**(4), 219.

72 C. W. Hsieh, R. K. Singh, M. L. Meena, S. A. Lu, K. K. Gupta, B. C. Lin and C. H. Lu, Development of inorganic perovskite quantum dots-based optical sensor for toxic Cd2+ metal ion detection, *Optik*, 2025, **22**, 172462.

73 X. Lao, X. Li, H. Ågren and G. Chen, Highly controllable synthesis and DFT calculations of double/triple-halide CsPbX3 (X= Cl, Br, I) perovskite quantum dots: application to light-emitting diodes, *Nanomaterials*, 2019, **9**(2), 172.

74 E. Stippell, P. C. Mora, N. Favate, L. Huang, C. W. Li and O. V. Prezhdo, Computational Screening of Ligands for Enhanced Interactions between Lead Halide Perovskite Quantum Dots, *J. Phys. Chem. Lett.*, 2025, **16**, 5666–5673.

75 D. Li, W. Xu, D. Zhou, X. Ma, X. Chen, G. Pan, J. Zhu, Y. Ji, N. Ding and H. Song, Cesium tin halide perovskite quantum dots as an organic photoluminescence probe for lead ion, *J. Lumin.*, 2019, **216**, 116711.

76 X. Sheng, Y. Liu, Y. Wang, Y. Li, X. Wang, X. Wang, Z. Dai, J. Bao and X. Xu, Cesium lead halide perovskite quantum dots as a photoluminescence probe for metal ions, *Adv. Mater.*, 2017, **29**(37), 1700150.

77 J. Sun, Q. Li, X. Li, C. Yan and G. Wang, Super stable and water-dispersible CsPbBr3 perovskite quantum dots for the efficient detection of Cu (II) and glutathione, *Microchem. J.*, 2024, **199**, 110043.

78 C. Gao, P. Yu, H. Yang, M. Wang, Y. Cao, J. Nie, W. Cao, M. Que, W. Zhu, P. Zhong and X. Ma, Enhanced photoluminescence and stability of CsPbBr3 quantum dots by anchoring on metal-organic frameworks for Cu2+ detection fluorescence probe, *J. Alloys Compd.*, 2025, **1023**, 180159.

79 S. Ahmed, S. Lahkar, S. Doley, D. Mohanta and S. K. Dolui, A hierarchically porous MOF confined CsPbBr3 quantum dots: fluorescence switching probe for detecting Cu (II) and melamine in food samples, *J. Photochem. Photobiol., A*, 2023, **443**, 114821.

80 P. He, W. Ge, Q. Zhang, M. Yang, H. Yin, X. Xie, Z. Luo and S. Shang, Eu3+ doped Cs–Bi–Cl perovskite quantum dots with diverse crystal structures for metal ion detection, *Ceram. Int.*, 2024, **50**(11), 20285–20292.

81 S. Ahmed, S. Lahkar, P. Saikia, D. Mohanta, J. Das and S. K. Dolui, Stable and highly luminescent CsPbX3 (X= Br, Br/Cl) perovskite quantum dot embedded into Zinc (II) imidazole-4, 5-dicarboxylate metal organic framework as a luminescent probe for metal ion detection, *Mater. Chem. Phys.*, 2023, **295**, 127093.

82 T. Vyas and A. Joshi, Chemical sensor thin film-based carbon quantum dots (CQDs) for the detection of heavy metal count in various water matrices, *Analyst*, 2024, **149**(4), 1297–1309.

83 Ö. Gencer, The production of carbon quantum dots (CQDs) from cultivated blue crab shells and their application in the optical detection of heavy metals in aquaculture, *Aquacult. Int.*, 2025, **33**(1), 107.

84 R. Üzek, Engineering a Graphene Quantum Dot-Enhanced Surface Plasmon Resonance Sensor for Ultra-Sensitive Detection of $Hg2^{+}$ Ions, *Adv. Mater. Interfaces*, 2025, **12**(5), 2400679.

85 P. Ayyanusamy, R. Venkatesan, A. N. Rajan, J. Annaraj, U. Mahalingam, P. Ramasamy, K. Bethke and J. Mayandi, Dimethylsulfoxide functionalized cadmium sulfide quantum dot for heavy metal ion detection, *Z. Phys. Chem.*, 2025, **28**, 121–134.

86 S. Iraqui, A. Dubey, I. Savarimuthu, A. Shankar, A. Jaiswal, I. Bahadur, I. Uddin and F. Mohammad, Bi-functional aqueous starch capped CdS quantum dots synthesis and their application as sensor of heavy metal-ions as well as photocatalytic dye degradation, *J. Mol. Liq.*, 2023, **388**, 122794.

87 D. Zhang, Y. Xu, Q. Liu and Z. Xia, Encapsulation of CH3NH3PbBr3 perovskite quantum dots in MOF-5 microcrystals as a stable platform for temperature and aqueous heavy metal ion detection, *Inorg. Chem.*, 2018, **57**(8), 4613–4619.

88 Y. Wang, Y. Zhu, J. Huang, J. Cai, J. Zhu, X. Yang, J. Shen and C. Li, Perovskite quantum dots encapsulated in electrospun fiber membranes as multifunctional supersensitive sensors for biomolecules, metal ions and pH, *Nanoscale Horiz.*, 2017, **2**(4), 225–232.

89 N. Ding, D. Zhou, G. Pan, W. Xu, X. Chen, D. Li, X. Zhang, J. Zhu, Y. Ji and H. Song, Europium-doped lead-free Cs3Bi2Br9 perovskite quantum dots and ultrasensitive Cu2+ detection, *ACS Sustain. Chem. Eng.*, 2019, **7**(9), 8397–8404.

90 M. T. Ahmed, D. Roy, A. A. Roman, S. Islam and F. Ahmed, C3B2 Quantum Dot: A Potential Candidate for Heavy Metal Ion Detection and Removal in Wastewater Treatment, *Langmuir*, 2025, **41**(14), 9456–9468.

91 H. Javeria, M. Q. Abbas, S. H. Chen, B. E. Keshat and Z. Du, Scalability of sulfur-functionalized carbon quantum dots from peanut shells: a sustainable sensor of high colorimetric heavy metal detection, *J. Environ. Chem. Eng.*, 2025, **13**(2), 115821.

92 J. Liu, Q. Zhang, W. Xue, H. Zhang, Y. Bai, L. Wu, Z. Zhai and G. Jin, Fluorescence characteristics of aqueous synthesized tin oxide quantum dots for the detection of heavy metal ions in contaminated water, *Nanomaterials*, 2019, **9**(9), 1294.

93 R. Yadav, V. Lahariya, S. A. K. Vikas, A. Das, A. Yadav and G. Gupta, Fluorometric sensing and nanomolar level detection of heavy metal ions using nitrogen doped carbon dots, *Emergent Mater.*, 2025, **8**(1), 363–377.

 © 2025 The Author(s). Published by the Royal Society of Chemistry

Open Access Article. Published on 23 October 2025. Downloaded on 10/25/2025 7:28:42 PM.
This article is licensed under a Creative Commons Attribution 3.0 Unported Licence.

94 P. Yadav and P. Chowdhury, Optical efficiency of CdTe QDs for metal ion sensing in the presence of different thiol-based capping agents, *Chem. Pap.*, 2022, **76**(3), 1833–1850.
95 M. Rana and K. Devlal, Thioglycolic Acid Capped CdTe Quantum Dots as Sensors for the Detection of Hazardous Heavy Metal Ion Cu 2+ in Water, *Mapan*, 2022, 1–6.
96 F. Farahmandzadeh, K. Kermanshahian, E. Molahosseini and M. Molaei, Efficient Mercury Ion Detection in Water: CdTe/CdS/ZnS Quantum Dots as a Simple, Sensitive, and Rapid Fluorescence Sensor, *J. Fluoresc.*, 2024, **13**, 1–2.
97 S. Sharma, P. Yadav and P. Chowdhury, Thioglycolic acid capped CdSe/ZnS quantum dot as fluorescent sensor for the detection of water-soluble hazardous heavy metal ions, *Appl. Phys. A:Mater. Sci. Process.*, 2024, **130**(5), 326.
98 K. He, X. Yu, L. Qin and Y. Wu, CdS QDs: facile synthesis, design and application as an "on–off" sensor for sensitive and selective monitoring Cu2+, Hg2+ and Mg2+ in foods, *Food Chem.*, 2022, **390**, 133116.
99 J. V. Rajendran, S. Parani, V. P. Remya, T. C. Lebepe, R. Maluleke, S. Thomas and O. S. Oluwafemi, Selective and sensitive detection of Cu2+ ions in the midst of other metal ions using glutathione capped CuInS2/ZnS quantum dots, *Phys. E*, 2022, **136**, 115026.
100 U. Latief, M. S. Khan, S. U. Islam, Z. Khan and M. A. Saifee, Environment friendly Co/Ag@ ZnS quantum dots with high quality emission and application for selective sensing of Hg2+, *J. Photochem. Photobiol., A*, 2023, **445**, 115038.
101 M. Kaur, S. Singh, S. K. Mehta, S. K. Kansal, A. Umar, A. A. Ibrahim and S. Baskoutas, CeO2 quantum dots decorated g-C3N4 nanosheets: a potential scaffold for fluorescence sensing of heavy metals and visible-light driven photocatalyst, *J. Alloys Compd.*, 2023, **960**, 170637.